FEDERAL UNIVERSITY OF PARÁ

GEOSCIENCES INSTITUTE

POST-GRADUATE PROGRAM IN GEOPHYSICS

Master 's Dissertation

Seismic physical modeling based on the physical similitudes: application in isotropic media

LEO KIRCHHOF SANTOS

BELÉM-PARÁ

2015

LEO KIRCHHOF SANTOS

Seismic physical modeling based on the physical similitudes: application in isotropic media

Master's thesis submitted to the Post-Graduate Program in Geophysics from Geosciences Institute-at Federal University of Pará for the obtainment of the title of Master in Geophysics

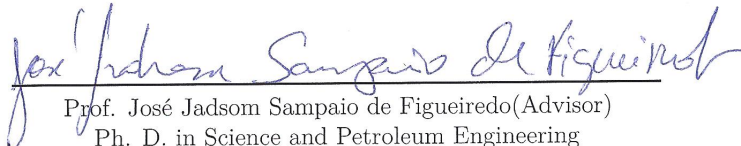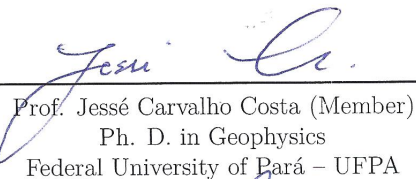Orientador: José Jadsom Sampaio de Figueiredo

BELÉM-PARÁ

2015

SEISMIC PHYSICAL MODELING BASED ON THE PHYSICAL SIMILITUDES: APPLICATION IN ISOTROPIC MEDIA
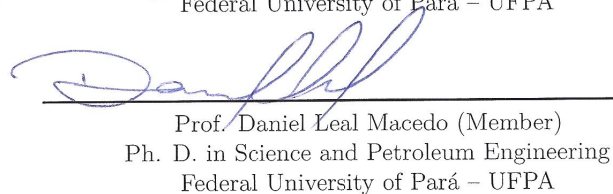
Leo Kirchhof Santos

Master's thesis submitted to the Post-Graduate Program in Geophysics from Geosciences Institute at Federal University of Pará for the obtainment of the title of Master in Geophysics

Approval Date : 02/12/2015
Grade: BOM(810), Aprovado
Committee Members:

Prof. José Jadsom Sampaio de Figueiredo(Advisor)
Ph. D. in Science and Petroleum Engineering
Federal University of Pará – UFPA

Prof. Jessé Carvalho Costa (Member)
Ph. D. in Geophysics
Federal University of Pará – UFPA

Prof. Daniel Leal Macedo (Member)
Ph. D. in Science and Petroleum Engineering
Federal University of Pará – UFPA

ACKNOWLEDGMENTS

RESUMO

Ao longo de décadas a modelagem física tem sido usada para ajudar geofísicos a entenderem os fenômenos relacionados a propagação de onda elástica em meios isotrópicos e anisotrópicos. A maioria dos trabalhos publicados relacionados a modelagem física utilizam similitudes físicas entre modelo e campo (ambiente geológico) apenas no contexto geométrico e, as vezes, no contexto cinemático. A similaridade dinâmica é aproximadamente ou, na maioria das vezes, não obedecida devido a dificuldade de reproduzir, em laboratório, as forças e tensões que existem no interior da Terra quando ocorre a propagação de ondas elásticas. Neste trabalho, uma expressão analítica para a similaridade dinâmica em meios isotrópicos é derivada em função da similaridade cinemática, impedância elástica e/ou dos parâmetros de Lamé (ou tensor de rigidez elástica) no contexto de tensão dinâmica (tensão gerada quando da propagação de uma onda). A expressão resultante para a similaridade dinâmica mostra que este tipo de similaridade possui múltiplas soluções no contexto da tensão dinâmica (problema de não unicidade). Entretanto, a regularização deste problema pode ser alcançada com o controle da porosidade e do conteúdo de argila. Medidas ultrassônicas (elásticas) assim como medidas petrofísicas (densidade e porosidade) em amostras de arenitos sintéticos mostram o quanto é difícil reproduzir em laboratório as três similitudes físicas estudadas neste trabalho. Outro importante resultado da análise feita neste trabalho foi alcançar uma expressão que relaciona a frequência da fonte sísmica com as fontes ultrasônicas usadas em laboratório.

Palavras-chave: Modelagem física. Similaridades físicas. Meios elásticos isotrópicos. Medidas ultrassônicas. Propagação de ondas elásticas.

ABSTRACT

Throughout the decades seismic physical modeling has been used to help the geophysicists to understand the phenomena related to the elastic wave propagation on isotropic and anisotropic media. Most of the published works related to physical modeling, use physical similitudes between model and field (geological environment) only in the geometric, and sometimes, in the kinematics sense. The dynamic similitude is approximately or, most of the time, not obeyed due to the difficulty to reproduce, in laboratory, the forces and tensions that exist inside the earth when elastic waves propagate. In this work, an analytical expression for dynamic similitude in isotropic media in the sense of dynamic stress (stress due wave propagation) was derived. The resulting expression for dynamic similitude shows that this type of similitude has multiple solutions in context of dynamic stress (non-unicity problem). However, the regularization of this problem can be reached by controlling porosity and clay content. Ultrassonic measurements(elastic) as well as petrophysical measurements (density, porosity and clay content) in synthetic sandstone samples show how difficult it is to reproduce in the laboratory the three physical similarities studied in this work. Other important result of our analysis (from the kinematic similitude), is the achievement of an expression that relates the seismic frequency source with ultrasonic sources which are used in laboratory.

Keywords: Physical modeling. Physical similarities. Isotropic elastic media. Ultrasonic measurements. Elastic wave propagation.

ILLUSTRATION LIST

TABLE LIST

SYMBOL LIST

Greek Symbols	Description
Ξ	Kinematic similitude
Σ	Dynamic similitude
Λ	Geometric similitude
σ	Stress tensor
ε	Strain tensor
μ	Shear modulus
λ	Wavelength
α	Physical parameters of fracture or cracks
ρ	Bulk density
ϕ	Porosity
ν	Particle velocity in the model

Latin Symbols	Description
n	Coefficient of porosity stress
K	Bulk modulus
M_{matriz}	Mass of the solid matrix
G_{dry}, G_{wet}	Shear modulus of the dry and saturated rock, respectivelly
F_1, F_2	Volumetric fraction of components 1 and 2, respectivelly
m/s	Unit of velocity: meters/seconds
km/h	Unit of velocity: kilometers/hours
g/cm^3	Density unit: gram/cubic centimeter
GPa	Unit of pressure: GigaPascal
MPa	Unit of pressure: MegaPascal
mD	Unit of permeability: mili-darcy
kHz	Unit of frequency: kiloHertz

SUMMARY

1 INTRODUCTION

There are basically three ways to generate seismic data in geophysical exploration community. The first one is the collection of seismic data from the field, a stage called seismic acquisition. In this case, there is low knowledge about the geological structures in subsurface and it is desirable to increase such knowledge through the analysis and interpretation of seismic data. The other two ways use generated synthetic data. They are called numerical modeling and physical modeling. In these cases, they need a prior knowledge about the geological model, or at least a strong set of model assumptions.

The numerical modeling assumes a geological model linked to more basic assumptions about the type of wave propagation. In this case, you can work with models for acoustic, elastic, viscoelastic, poroelastic or seismelectric medium (CARCIONE; HERMAN; KROODE, 2002; NAKAGAWA; SCHOENBERG, 2007; SCHAKEL et al., 2011; VAVRYUK, 2008). Furthermore, for numerical modeling, it should be provided numerical data on the parameters that configure the model chosen, thus, in the end of the process, the created model is as realistic as possible. After the choice of the model, the numerical method to simulate the wave propagation should be chosen. For this step, there is a wide variety of options, such as: ray tracing, or finite differences, elements and volume, among others (CARCIONE; HERMAN; KROODE, 2002; VIRIEUX; CALANDRA; PLESSIX, 2011).

Due to numerical dispersion problems that can be found in the modeling of cracks and fractures (COATES; SCHOENBERG, 1995; ZHANG, 2005), what is usually done in numerical modeling is the replacement of cracks and fractures by an effective medium. However, the individual effect of fractures or cracks can not be modeled satisfactorily (SAENGER; SHAPIRO, 2002). In physical modeling this problem is not found, since cracks and fractures can be physically simulated by materials having a very low shear modulus (e.g. rubber disks or rubber strips peaces) with different physical characteristics (ASSAD et al., 1993; ASSAD et al., 1996; FIGUEIREDO et al., 2012; FIGUEIREDO et al., 2013; SANTOS et al., 2015). Cracks and fractures may also be represented by empty spaces in a homogeneous solid matrix (HUANG; STEWART; DYAUR, 2014; OMOBOYA et al., 2015; STEWART et al., 2011) as well as in a synthetic porous matrix (RATHORE et al., 1995; TILLOTSON et al., 2011; WANG et al., 2015).

A feasible seismic modeling, whether physical or computational, is a necessary tool to all stages of the seismic survey (CARCIONE; HERMAN; KROODE, 2002). For example, the use of preliminary information on the seismic acquisition stage in a computational modeling can be used to properly configure the seismic experiment in accordance with the local geology, providing better illumination of targets of interest. In the signal processing

Table 1.1 – Velocities (P and S wave) and density values of common materials used in the construction of seismic physical modeling.

Medium material	Type of medium	Dry Vel. V_P (m/s)	Dry Vel. V_S (m/s)	Bulk Density ρ (kg/m^3)
Steel (EBROM; MCDONALD, 1994)	Isotropic	5900	3260	7800
Aluminium (EBROM; MCDONALD, 1994)	Isotropic	6400	3150	2700
Brass (EBROM; MCDONALD, 1994)	Isotropic	4300	2100	8500
Copper (EBROM; MCDONALD, 1994)	Isotropic	4700	2260	8900
Lucite Bulk (HSU; SCHOENBERG, 1993)	Isotropic	2725	1368	1364
Plexiglass Bulk (ALHUSSAIN; GUREVICH; UROSEVIC, 2008)	Isotropic	2724	1384	1200
Phenolic CE Bulk (CHEADLE; BROWN; LAWTON, 1991)	Anisotropic	2925*	1610**	1364
Epoxy Resin (solid) (ASSAD et al., 1996)	Isotropic	2600	1181	1040

* compressional-wave velocity parallel to bedding plane.
** shear-wave velocity parallel to bedding plane.

step, such modeler can be used to validate and adjust the methods used during this step. Also, during the data interpretation, it can be used to compare different geological hypotheses about the model from the observed difference between predicted and existing seismic data.

Table 1.1 shows common materials generally used to create scaled model in laboratory. An experimental work performed by French (1974), French (1975) was important to show that the image of complex structures requires a 3D imaging processing. The synthetic model constructed by French (1974) received his name and was constructed with artificial materials such as rubber and epoxy resin. Recently, Tantsereva et al. (2014), based on French's model (FRENCH, 1974), constructed the Marsille model. In this work they tested benchmarking of 3D numerical methods with experimental approach. To construct the Marsille model they used PVC (Polyvinyl chloride) as the raw material. It is worthy to say that Cheadle, Brown e Lawton (1991), Hsu e Schoenberg (1993), Assad et al. (1996), Figueiredo et al. (2013), Figueiredo et al. (2012) and Far et al. (2014) performed significative studies and analyses in anisotropic physical model using synthetic material like those described in Table 1.1.

Although the experiments cited here were very useful to improve numerical techniques in seismic processing, they have some limitations when trying to work with the 4D time-lapse method. For example, the materials listed in Table 1.1 show a null porosity and, in bulk condition (it means no laminar or layered), show invariance with triaxial confining stress. To create a scaled model in laboratory with similar characteristics of geological en-

vironment it is necessary to use natural materials like sand, clay, etc. Sherlock, McDonald e Evans (1997) created a physical model based on sand (main ingredient). This model was called sandbox model (SHERLOCK; MCDONALD; EVANS, 1997; SHERLOCK; EVANS, 2001). Among others objectives, they used this model to investigate the mechanisms related to oil migration in sandstone reservoir. Using sand and epoxy Rathore et al. (1995) and Tillotson et al. (2011) also created synthetic sandstones with pore structure similar that one found in the real rocks. Using natural carbonates, epoxy resin and silicone rubber discs Wang et al. (2015) created synthetic carbonates rocks.

The main goal of this work is to analyze the formalisms of physical similitudes (BUCKINGHAM, 1914; KLINE, 1986; MARGHITU, 2001; TEODORESCU, 2007) in the context of elastic wave propagation. Also, it is attempted to create a simplified mathematical formalism for dynamic similitude context. This expression is analitically and experimentally analyzed. Isotropic synthetic samples with different concentration of cement, sand and clay were constructed. P- and S- velocities, density and porosity measurements were performed for experimentally analyze this new formalism of dynamic similitudes. Furthermore, it is derived an expression that relates the source frequency in the field with the source frequency used in laboratory. First, a briefly explanation about the physical similitudes is realized. After this, the process of production of the synthetic rocks and estimative of their elastic and petrophysical properties is described. Later, the mathematical formalisms are analitically described and the dynamic similitude is experimentally analyzed.

It is necessary to point out that this work has a format of paper, hence, it will be necessary to reduce its size when the process of submission begins. The idea is to divide the present work in two different parts: a theoretical analysis, involving all the mathematical formalisms and analytical analyses, and a experimental analysis, showing all the process of production of synthetic rocks realized in laboratory and the physical analyses involving them.

2 THEORETICAL BACKGROUND

2.1 Physical similitudes

Physical modeling is defined as the ability to simulate the physical aspects of a natural scenario (large-scale) on an environment of reduced scale. In this approach, the main goal is to reproduce the behavior of the physical properties (geometric, kinematic and dynamic), displayed by a full-scale environment, in a reduced scale model (BUCKINGHAM, 1914; KLINE, 1986). In the seismic context, more specifically in the hydrocarbon reservoir scenario, the elastic properties of the physical models reproduced in laboratory must have the highest fidelity in comparison to those shown by geological structures in the subsurface.

In the following description, it is always refered to the seismic context as a field context using the letters 'f' (field) and 'm' (model) to specify the full-scale and prototype environments respectively.

2.1.1 Geometric similitude

Generally, the scale effect of a specific phenomenon (in our case, a geologic phenomenon) increases according to the following scale ratios or scale factors (HUGHES, 1993; HELLER, 2011) for length (L), area (A) and volume (V),

$$\Lambda = \frac{L^{(f)}}{L^{(m)}}, \tag{2.1}$$

$$\Lambda^2 = \frac{(L^{(f)})^2}{(L^{(m)})^2} = \frac{A^{(f)}}{A^{(m)}}, \tag{2.2}$$

$$\Lambda^3 = \frac{(L^{(f)})^3}{(L^{(m)})^3} = \frac{Vol^{(f)}}{Vol^{(m)}}, \tag{2.3}$$

where $L^{(f)}$ is the characteristic length in the field and $L^{(m)}$ is the corresponding length in the model. The scale factor of equation (2.1) in terms of proportion is defined by 1: Λ. The size of the model, time and the construction cost increase with the increasing of Λ^{-1} (BUCKINGHAM, 1914; HELLER, 2011; KLINE, 1986). In other words, the parameter Λ is related to the criteria of mechanic similitude called geometric similitude. Besides this type of similitude, two other types are outstanding in the physical modeling context: the kinematic and dynamic similitudes. The first one implies the similitude of the particles motion (velocity and acceleration) between the model and the geological structure. The second one is the ratio of forces in the field and in the model, which can be static (overburden) or dynamic.

Figure 2.1 – Seismic physical modelling in context of geometric and kinematic similitude. The scale change is a result of distance upscale and frequency downscale from laboratory to field.
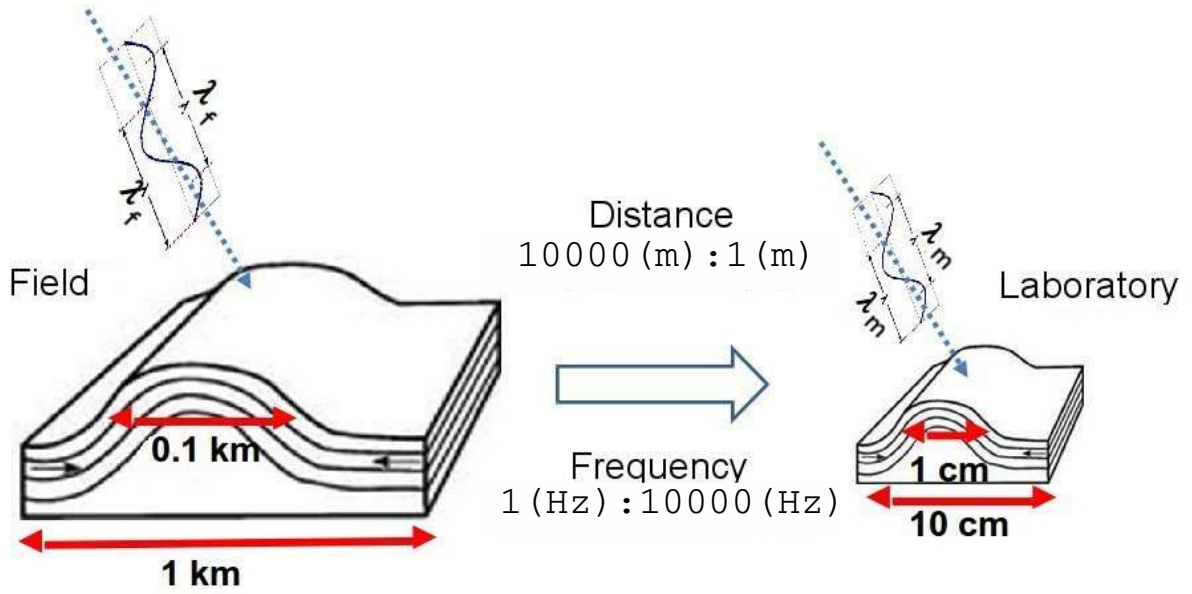
Source: From author.

Figure 2.1 shows how the scale change is performed from geological background to seismic physical model. An anticline structure is used as example. In the field, this kind of structure can have sizes in the order of kilometers or hundreds of meters. To model this structure in laboratory, it is initially needed to find the geometric similitude factor affordable to construct this model, taking into account the economic and time construction issues. In this case, an affordable scale factor between field and model would be 10000:1. Second, it is necessary to find the better fit of seismic frequency with the ultrasonic frequency in the laboratory to perform the data acquisition. In the next section, it is showed that, unlike the length scale, the frequency suffers an upscale of frequency content. In the case of the example of Figure 2.1, the scale change is 1:10000. It means that each Hz in seismic is equivalent to 10000 Hz.

2.1.2 Kinematic similitude

The kinematic similitude is mathematically written by (MARGHITU, 2001; TEODORESCU, 2007),

$$\Xi_V = \frac{V^{(f)}(x,y,z)}{V^{(m)}(x,y,z)}, \tag{2.4}$$

and

$$\Xi_\nu = \frac{||\nu^{(f)}(x,y,z)||}{||\nu^{(m)}(x,y,z)||} \tag{2.5}$$

where $V^{(f)}(x,y,z)$, $V^{(m)}(x,y,z)$ are the seismic velocities (interval velocities) in the field and in the model and $\nu^{(f)}(x,y,z)$ and $\nu^{(m)}(x,y,z)$ are the particle velocity in the field

and in the model, respectively. It is worthy to mention that these velocities are related to the modes of vibration, P, S or converted wave velocities (in tridimensional space). This ratio can also be used as a scale factor of traveltime between the real seismic section and a seismic section from the model (FRENCH, 1974).

2.1.3 Dynamic similitude

This type of similitude is the ratio between field forces and model forces. In the case of seismic or seismology, the effect of forces is related to the stress tensor that can be dynamic or static. Based on these behaviors, the dynamic similitude is divided in two different approaches.

First, for the static point of view, the effective stress (σ_{eff}) in a natural porous rock beneath the earth's surface is given by (CARCIONE et al., 2003; ZIMMERMAN, 1990)

$$\sigma_{eff} = S - \alpha P^{pore}, \tag{2.6}$$

where S, P^{pore} and α are the confining pressure, pore pressure and effective stress coefficient (dimensionless), respectively. According to the compressibility measurement performed by (ZIMMERMAN, 1990), α is considered ≈ 1.

In this way, the dynamic similitude parameter associated to the static stress is given by

$$\Sigma_s = \frac{\sigma_{eff}^{(f)}}{\sigma_{eff}^{(m)}} = \frac{S^{(f)} - P^{pore(f)}}{S^{(m)} - P^{pore(m)}}. \tag{2.7}$$

In the case of dry rocks, the equation (2.7) becomes

$$\Sigma_s \approx \frac{S^{(f)}}{S^{(m)}}. \tag{2.8}$$

In expressions (2.7) and (2.8) the static dynamic similitude can be attended ($\Sigma_s = 1$) if a high pressure ultrasonic equipment is used in order to submit the sample to high confining pressure with controlled pore pressure environment.

Second, now considering the dynamic similitude in the dynamic stress context, the definition of stress as a function of stiffness elastic coefficients (C_{ijkl}) and strain tensor (ε_{kl}) is given by:

$$\sigma_{ij}^{(f)} = C_{ijkl}^{(f)} \varepsilon_{kl}^{(f)}, \tag{2.9}$$

for field and

$$\sigma_{ij}^{(m)} = C_{ijkl}^{(m)} \varepsilon_{kl}^{(m)}, \tag{2.10}$$

for model. It is known that the dynamic stiffness elastic coefficients (C_{ijkl}) depends on the Lamè parameters K and μ.

$$C_{ijkl}^{(f)} = C_{ijkl}^{(f)}(K^{(f)}, \mu^{(f)}), \tag{2.11}$$

$$C_{ijkl}^{(m)} = C_{ijkl}^{(m)}(K^{(m)}, \mu^{(m)}), \tag{2.12}$$

wher K and μ are the rock and model bulk modulus and shear modulus, respectively.

In the seismic context, these parameters depend on P-wave velocity, S-wave velocity and density, such as:

$$K^{rock} = K^{rock}(V_P, V_S, \rho), \tag{2.13}$$

$$\mu^{rock} = \mu^{rock}(V_P, V_S, \rho) \tag{2.14}$$

In the geological context, velocities and density also depend on other physical parameters, such as:

$$V_P^{rock} = V_P^{rock}(\phi, T, V_{clay}, \zeta, \sigma_{eff}, \kappa), \tag{2.15}$$

$$V_S^{rock} = V_S^{rock}(\phi, T, V_{clay}, \zeta, \sigma_{eff}, \kappa), \tag{2.16}$$

$$\rho^{rock} = \rho^{rock}(\rho_{matrix}, \phi, S_{fluid}, \kappa), \tag{2.17}$$

where ϕ, T , V_{clay}, ζ, p_{eff}, ρ_{matrix}, κ and S_{fluid} correspond to porosity, temperature, clay volume, physical parameters of fracture or cracks (aspect-ratio, crack density, etc), effective pressure, matrix density (grain density), permeability and fluid content in pores. For now the analysis of this third type of similitude is considered only in the context of velocity and density. Later, it will be highlighted these physical and petrophysical parameters that affect the velocity and density magnitude in the rocks.

The dynamic similitudes for dynamic stress/strain relation, in terms of Lamè parameters, are given respectively

$$\Sigma_d^p = \frac{K^f}{K^m} = \frac{(\rho V_p^2 - \frac{4}{3}\rho V_s^2)^f}{(\rho V_p^2 - \frac{4}{3}\rho V_s^2)^m}, \tag{2.18}$$

and

$$\Sigma_d^s = \frac{\mu^f}{\mu^m} = \frac{(\rho V_s^2)^f}{(\rho V_s^2)^m} \tag{2.19}$$

where K and μ are, respectively, bulk modulus and shear modulus. Reorganizing equation 2.18 putting ρ and V_s in evidence

$$\Sigma_d^p = \frac{(\rho^f V_s^{2f})(\frac{V_p^2}{V_s^2} - \frac{4}{3})^f}{(\rho^m V_s^{2m})(\frac{V_p^2}{V_s^2} - \frac{4}{3})^m} \tag{2.20}$$

It is possible to express equation 2.20 in terms of S-wave dynamic similitude (2.19) and the ratio of V_p and V_s (α) in the following way

$$\Sigma_d^p = \Sigma_d^s \frac{(\alpha^2 - \frac{4}{3})^f}{(\alpha^2 - \frac{4}{3})^m} \tag{2.21}$$

3 EXPERIMENTAL PROCEDURE

3.1 Sample preparation

This chapter presents the experimental procedure for construction as well as the ultrasonic measurements in the sandstones synthetic samples. The main goal of these samples construction is to verify, in controlled conditions, the feasibility of new analytical expression of dynamic similitude presented in the last chapter. The construction of the synthetic samples as well as the ultrasonic measurements was carried out at the Laboratory of Petrophysics and Rock Physics Dr. Om Prakash Verma (LPRP), at Federal University of Pará, Brazil. Under controlled conditions, it was constructed twenty six sandstones samples, divided in three groups. In the first group, the samples were made of sand and cement with loss of material during the construction, while the second and third group without loss of material during the construction. The third group are shaly-sandstone made based on cement, clay and sand and without loss material during the construction.

3.1.1 Synthetic sandstones

Initially, the grains of the rocks (sand, clay and cement) used to create the samples were mixed in a recipient until they become a homogeneous powder mixture. After this, water was inserted in the mixture in order to transform it in a viscous mass, which was then put into a cylindrical mould, consisting of a sliced piece of PVC pipe. This process was repeated for each sample of the groups. The same concentration of water was used for each sample group. The main difference between sample of group 1 and samples of group 2 and 3 is that in these last two groups, only a small amount of water was added in the stage of mixing of materials. This fact caused almost zero loss of material when pressure was applied to the mixture, while for group 1 the loss of material was very high, because of the high amount of water used. Later, it will be showed how this fact influence in the behaviour of the elastic and petrophysical properties of these samples. After this, all the samples were submitted to a constant static press of approximately 10 MPa, made by a hydraulic press (see Figure 3.1). The final stage of the construction process was to place the samples into an heater device in order to get them dry.

The first group is composed by cemented sandstone samples with seven different cement concentration, ranging from 25% to 70% while the second group the samples have nine different cement concentration samples, ranging from 10% to 70%. In addition to these sandstones, a sample composed by 100% of cement was created to act as a reference sample. The third group is composed by nine different samples with with varying

Figure 3.1 – Picture of the hydraulic press that is used to simulate de overburden effect in the samples.

Source: From author

Figure 3.2 – Pictures of the group samples: a) group AA, b) group 3A, and c) group E. Their composition and elastic properties are described in Tables 3.4, 3.5 and 3.6.

(a)

(b)

(c)
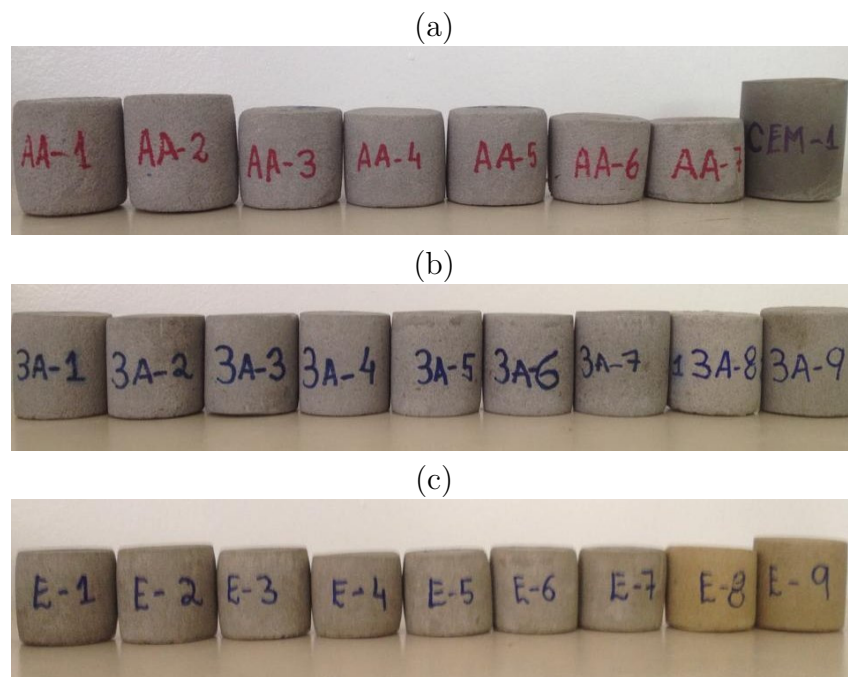
Source: From author

concentration of cement and clay, and a fixed concentration of 60% of sand. Figures 3.2 shows the samples labeled from AA-1 to AA-7 in the case of first group, 3A-1 to 3A-9 in the case of second group and from E-1 to E-9 in the third group and Cem-1 in the case of the cement sample. Beyond the differences in composition and concentration of cement, the samples have different dimensions and porosity. Physical characteristics of all the samples are showed in Tables 3.1, 3.2, 3.3, 3.4, 3.5 and 3.6.

Table 3.1 – Physical parameters (length, diameter and mass) of the synthetic samples AA. All the samples were submitted to a effective pressure of 10 MPa.

Type of artificial rock	Length (cm)	Diameter (cm)	mass (g)
Sample AA-1	3.93	3.81	80.68
Sample AA-2	3.98	3.8	87.82
Sample AA-3	3.52	3.78	78.42
Sample AA-4	3.4	3.8	81.63
Sample AA-5	3.47	3.84	82.17
Sample AA-6	3.1	3.7	64.91
Sample AA-7	2.95	3.7	60.87
Sample Cem-1	4.49	3.83	98.18

Source: From author.

Table 3.2 – Physical parameters (length, diameter and mass) of the synthetic samples 3A. All the samples were submitted to a effective pressure of 10 MPa.

Type of artificial rock	Length (cm)	Diameter (cm)	mass (g)
Sample 3A-1	4.17	3.84	94.23
Sample 3A-2	4.06	3.85	97.79
Sample 3A-3	4.06	3.87	99.96
Sample 3A-4	4.08	3.85	102.44
Sample 3A-5	4.17	3.86	103.15
Sample 3A-6	4.03	3.86	101.37
Sample 3A-7	4.14	3.86	103.63
Sample 3A-8	4.1	3.83	77.4
Sample 3A-9	4.17	3.83	85.34

Source: From author.

3.2 Ultrasonics measurements

The ultrasonics measurements were performed using the Ultrasonic Research System at LPRF with the pulse transmission technique. The sampling rate per channel for all measures of P and S-wave records was 0.1 μs. Figure 3.3 shows the experimental setup of the ultrasonic system used in this work. The system is formed by: a pulse-receiver 5072PR and pre-amplifier 5660B from Olympus, a USB oscilloscope of 50 MHz from Handscope and P and S-wave transducers of 1 MHz also from Olympus.

Figure 3.4 shows the device developed for recording P-wave and S-wave seismograms, with rotating polarization for both. The source and receiver transducers were arranged on opposing sides of the samples, separated by the length of the sample measured. To

Table 3.3 – Physical parameters (length, diameter and mass) of the synthetic samples E. All the samples were submitted to a effective pressure of 10 MPa.

Type of artificial rock	Length (cm)	Diameter (cm)	mass (g)
Sample E-1	3.66	3.84	86.42
Sample E-2	3.75	3.85	89.7
Sample E-3	3.6	3.84	84.52
Sample E-4	3.39	3.85	79.97
Sample E-5	3.41	3.81	80.4
Sample E-6	3.51	3.84	84.99
Sample E-7	3.46	3.85	81.64
Sample E-8	3.47	3.82	78.2
Sample E-9	3.78	3.85	90.64

Source: From author.

ensure the propagation of wave was in the desired region of the samples, the transducers were placed at the center of either side. The velocities were measured in the longitudinal direction of the samples.

This transmission measurements were performed using a S-wave high frequency transducer only. This type of transducer allows to acquire the traveltimes of both P and S-waves from a single waveform. These transducers have an intrinsic delay time of $0.14\mu s$ in its signal, being necessary to take this delay into consideration when estimating the waves velocities. The P and S-wave velocities were estimated and their respectivity values are depicted in Tables 3.4, 3.5 and 3.6. Figure 3.5a shows the P and S- source wavelet pulse of transducers which are present in this laboratory. The peak frequency of the P and S transducers, as can be seen in Figure 3.5b, is around 1 MHz.

3.3 Porosity estimation

Another property of the samples estimated in this work was porosity. The values for all the samples are approximated values, since the process os measure was rustic. The samples were immerse in distilled water, which has density equals $1g/cm^3$, until become totally filled with the fluid. As the water density is considered 1, the volume occupied by the water in the pores is the same as the mass added to the sample after being immersed. Dividing this volume by the total volume of the rock it was possible to estimate the porosity of the samples in terms of percentage. Measure of all sample's porosities are shown in Tables 3.4, 3.5 and 3.6.

Figure 3.3 – The experimental setup for P- and S- waveform acquisition.
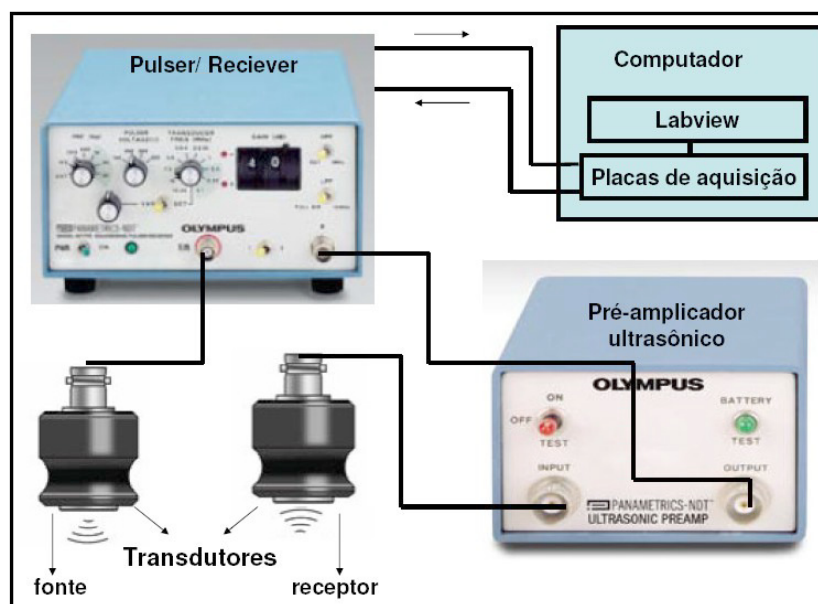
Source: From author

Figure 3.4 – Equipment developed in this laboratory for the acquisition of transmitted ultrasonic waves for P- and S- waves modes.
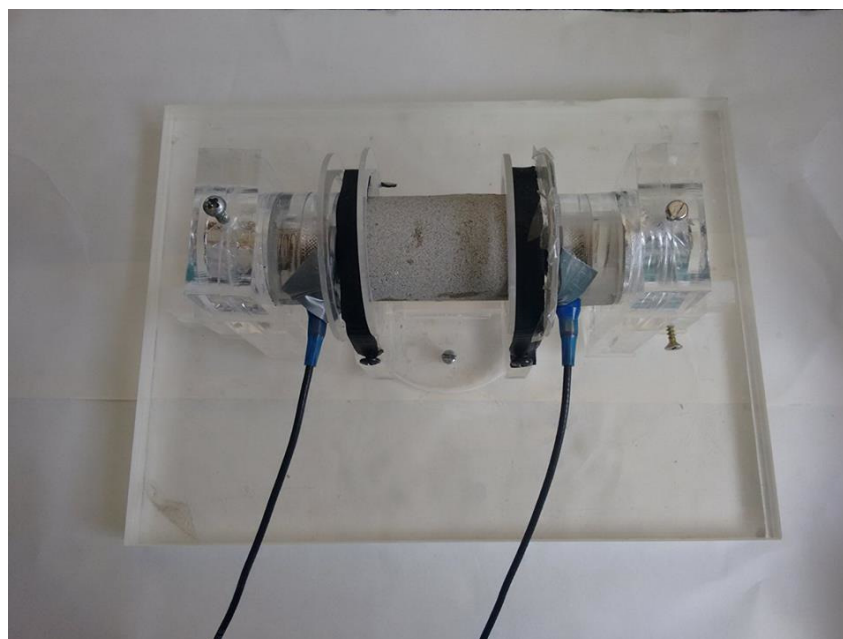
Source: From author

Figure 3.5 – a) The source signatures of P- and S-wave transducer. The non zero first arrival shows the intrinsic delay time of transducers. b) Frequency spectra of the P and S-waveforms. As can be noted, the peak frequency is around 1MHz.

(a)

(b)
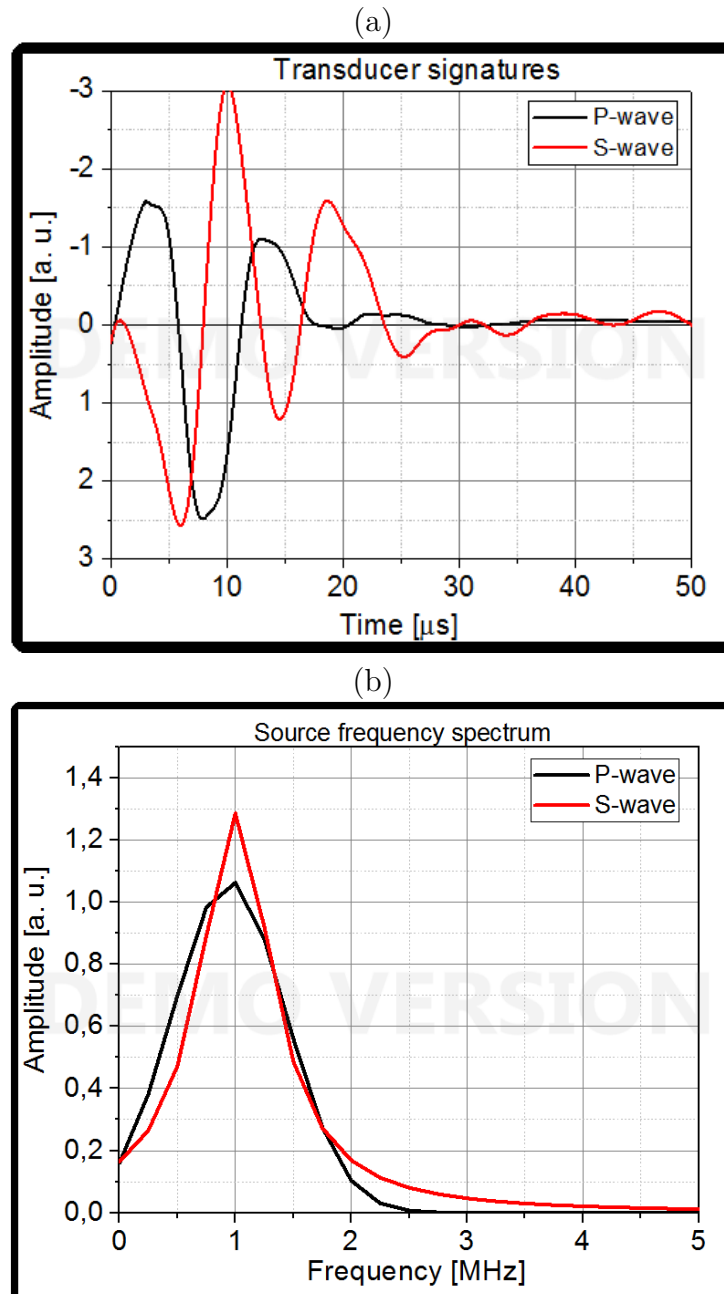
Source: From author

Table 3.4 – Elastic and petrophysical properties of synthetic samples composed of sand and cement (group 1).

Type of artificial rock	Dry Vel. V_P (m/s)	Dry Vel. V_S (m/s)	Bulk Density ρ (kg/m^3)	Cement Concentration %	Porosity (%)
Sample AA-1	2200	1436	1800	25	15.1
Sample AA-2	2432	1703	1945	35	16.6
Sample AA-3	2634	1772	1986	45	15.8
Sample AA-4	2992	2143	2116	50	14.5
Sample AA-5	2925	1738	2044	60	14.6
Sample AA-6	2263	1643	1947	65	20.3
Sample AA-7	1985	1381	1919	70	22.6
Sample Cem-1	3409	2162	1890	100	≈ 0

Source: From author.

Table 3.5 – Elastics and petrophysical properties of synthetic samples composed of sand and cement (group 2).

Type of artificial rock	Dry Vel. V_P (m/s)	Dry Vel. V_S (m/s)	Bulk Density ρ (kg/m^3)	Cement Concentration %	Porosity (%)
Sample 3A-1	1718	894	1638	10	26
Sample 3A-2	2008	1524	1776	15	23.8
Sample 3A-3	3183	2219	1950	25	9.58
Sample 3A-4	3355	2312	2060	35	8.7
Sample 3A-5	3548	2553	2090	45	5.65
Sample 3A-6	3669	2700	2150	50	5.72
Sample 3A-7	3645	2569	2110	60	5.69
Sample 3A-8	3704	2697	2140	65	5.5
Sample 3A-9	3767	2709	2130	70	6.62

Source: From author.

Table 3.6 – Elastic and petrophysical properties of synthetic samples composed of sand, cement and clay (group 3). All the samples were submitted to an effective pressure of 10 MPa.

Type of artificial rock	Dry Vel. V_P (m/s)	Dry Vel. V_S (m/s)	Bulk Density ρ (kg/m^3)	Clay Content %	Cement Concentration(%)	Porosity (%)
Sample E-1	1176	756	1966	30	10	15.79
Sample E-2	2171	1469	2059	25	15	14.65
Sample E-3	2743	1577	2037	4	36	13.1
Sample E-4	2727	1521	2053	5	35	13
Sample E-5	2591	1523	2025	6	34	12.9
Sample E-6	2591	1345	2024	7	33	12.1
Sample E-7	2432	1378	2065	8	32	13.4
Sample E-8	2394	1367	2100	9	31	13.42
Sample E-9	2243	1352	2025	10	30	13.4

Source: From author

4 RESULTS

4.1 Theoretical analyses

In this chapter, it will be discussed the more important types of similitudes on physical modeling, in other words, kinematic and dynamic similitude. The geometric similitude will not be considered since it has already been contemplated in Chapter 2. Beyond that, the experimental results about synthetic sandstones are shown in order to compare model sample with real plug rocks.

4.1.1 Kinematic similitude and frequency scaling factors

Considering that the velocity inside each layer is constant (long wavelength approximation), phase velocities (V_P and V_S) definition of field can be used

$$V^{(f)} = \lambda^{(f)} f^{(f)}, \tag{4.1}$$

and model

$$V^{(m)} = \lambda^{(m)} f^{(m)} \tag{4.2}$$

where $\lambda^{(f)}$ and $\lambda^{(m)}$ are the wavelengths in the field and in the model and $f^{(f)}$ and $f^{(m)}$ are the dominant frequencies in the field and in the model. From equations (4.1) and (4.2), the kinematic similitude factor between the field and the model can be written by

$$\Xi_V = \frac{V^{(f)}}{V^{(m)}} = \frac{\lambda^{(f)} f^{(f)}}{\lambda^{(m)} f^{(m)}}. \tag{4.3}$$

Considering that elastic velocities between the model and the field can be, in most of the cases, close to each other (assuming that it was found a specific material with the same field velocity) or sometimes equal, from equation (4.3)

$$f^{(m)} = \left(\frac{\lambda^{(f)} f^{(f)}}{\lambda^{(m)}} \right) \times \text{constant} \tag{4.4}$$

where the dominant frequency bandwidth in the field can vary from 0 to 250 Hz (HEARN; HENDRICK, 2001; CARTER; PAMBAYUNING, 2009). This proportionality constant is approximately 1 for case in which the velocity of model is very similar to the field. In case of a physical model that simulates a geological formation with N layers this constant can be expressed by the average of the kinematic similitude for N layers, i. e.,

$$\text{constant} = \sum_{i=1}^{N} \frac{V_i^{(f)}}{V_i^{(m)}} \frac{1}{N}. \tag{4.5}$$

The registered frequency will depend on the type of the rock formation and several factors that can influence the seismic frequency bandwidth. For seismic velocity, according to (BOURBIÉ; COUSSY; ZINSZNER, 1987), sedimentary rock velocities can be in intervals of 300 to 6500 m/s. Considering that the size of seismic physical model is generally on the order of 10^{-1} to 10^{1}m (BARRIÈRE et al., 2012; FRENCH, 1974; MAHMOUDIAN et al., 2015; SHERLOCK; EVANS, 2001; STEWART et al., 2011), it is assumed that the dominant wavelength in the model should be on the order of 10^{-2} to 10^{-1}m (effective wavelength).

In terms of magnitude values, the parameters f_f, λ_f and λ_m will vary with $1 \leq a \leq 2$ and $0 \leq b \leq 1$, respectively. This can also be mathematically present as:

$$f^{(f)} \sim 10^{a} \text{ Hz} , \tag{4.6}$$

$$\lambda^{(f)} \sim 10^{\frac{2}{a}} \text{ m} , \tag{4.7}$$

$$\lambda^{(m)} \sim 10^{-b-1} \text{ m} . \tag{4.8}$$

In this way, equation (4.4) can be written in terms of order of magnitude from equations (4.6), (4.7), (4.8)

$$f^{(m)} \sim (10^{[a+\frac{2}{a}+b+1]} Hz) \times \text{constant}, \tag{4.9}$$

which, in the case of the model, the following frequency intervals should deal in the following magnitude order

$$f^{(m)} \sim 10^{4} \text{ Hz} \qquad \text{if} \quad a = 1 \quad \text{and} \quad b = 0, \tag{4.10}$$

$$f^{(m)} \sim 10^{5} \text{ Hz} \qquad \text{if} \quad a = 1 \quad \text{and} \quad b = 1, \tag{4.11}$$

$$f^{(m)} \sim 10^{6} \text{ Hz} \qquad \text{if} \quad a = 2 \quad \text{and} \quad b = 1. \tag{4.12}$$

It is worthy to say that these values are the optimal values to perform frequency scale transfer from field to model, since the geometric and kinematic similitude had been satisfied. Considering that the dominant frequencies of the ultrasonic transducers used in physical modeling laboratories vary from 50 kHz (MARION; MUKERJI; MAVKO, 1994) to 5 MHz (STEWART et al., 2011), it can be affirmed, from equation system (2.1-2.3) and equation (4.9), that the process of physical modeling happens through an upscaling in the distance scale and a downscaling in the frequency as shown in Figure 2.1.

Figure 4.1 shows the wavelengths ranging in the field and in the model using values of the sedimentary rock velocities interval proposed by (BOURBIÉ; COUSSY; ZINSZNER, 1987) and source frequency bandwidth in field (CARTER; PAMBAYUNING, 2009; HEARN; HENDRICK, 2001) and in model (MARION; MUKERJI; MAVKO, 1994; STEWART et al., 2011). Scale frequencies of Figures 4.1 c) and d) were reduced to the usual dominant frequencies of seismic sections from field and laboratory.

Figure 4.1 – Possible wavelength values related to seismic velocity (a) and similar model velocity (b). Using usual frequency interval for field (c) and model (d) after passing through medium or material, the high frequency is attenuated and the registered signal show a reduction in the frequency interval.
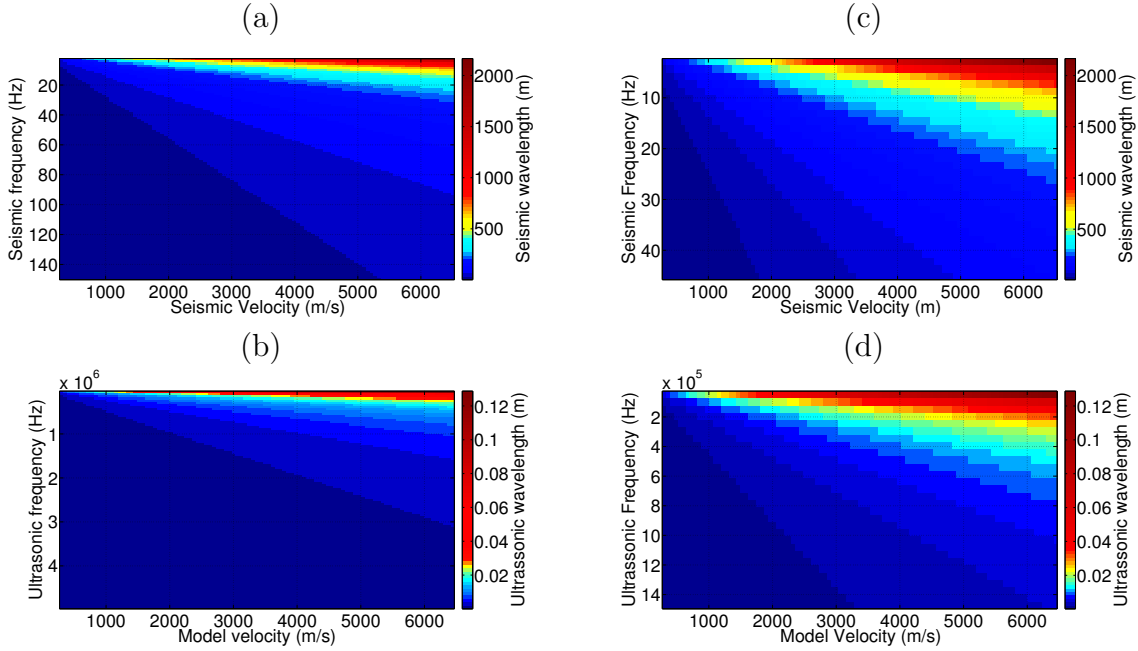
Source: From author

4.1.2 Dynamic similitude from static stress

As mentioned above, the dynamic similitude in seismic context is divided in two types of similitudes. Regarding the external stress condition (dynamic similitude in static context), with an adequate high-pressure equipment (ultrasonic), it is possible to reach a pressure similar to the one in the subsurface. Figure 4.2 shows P- and S-wave velocities and density well logs from Norne field-Norway (well 660810-B-4AH) as well as the overburden stress (S_{over}) as a function of depth (z) estimated by (CARCIONE et al., 2003)

$$S_{over}(z) = S_{over}(z_0) + g \int_{z_0}^{z} \rho(z)dz \qquad (4.13)$$

where g is the gravitational acceleration constant, z_0 is the initial depth and $\rho(z)$ is the density.

It is worthy to mention that the effective pressure expressed by equation (4.13) is not displayed in Figure (4.2 d). There are several methods used to estimate the pore pressure in a reservoir, even from seismic (CARCIONE et al., 2003) as well as from well-log (ZHANG, 2011) datasets. As shown in equation (2.6), the pore-pressure tends to decrease the effective pressure. Considering this, it is correct to affirm that most of high-pressure equipments (ultrasonic) can provide enough pressure to keep a similar static stress magnitude from a great number of hydrocarbon reservoir in the field e.g., (SUN; HAN; BATZLE, 2009; VERNIK; NUR, 1992).

Figure 4.2 – (a) P-wave velocity, (b) S-wave velocity and (c) density well logs from Norne field-Norway (well 660810-B-4AH). The overburden pressure (d) was calculated based on equation (4.13).

(a)

(c)

(b)

(d)
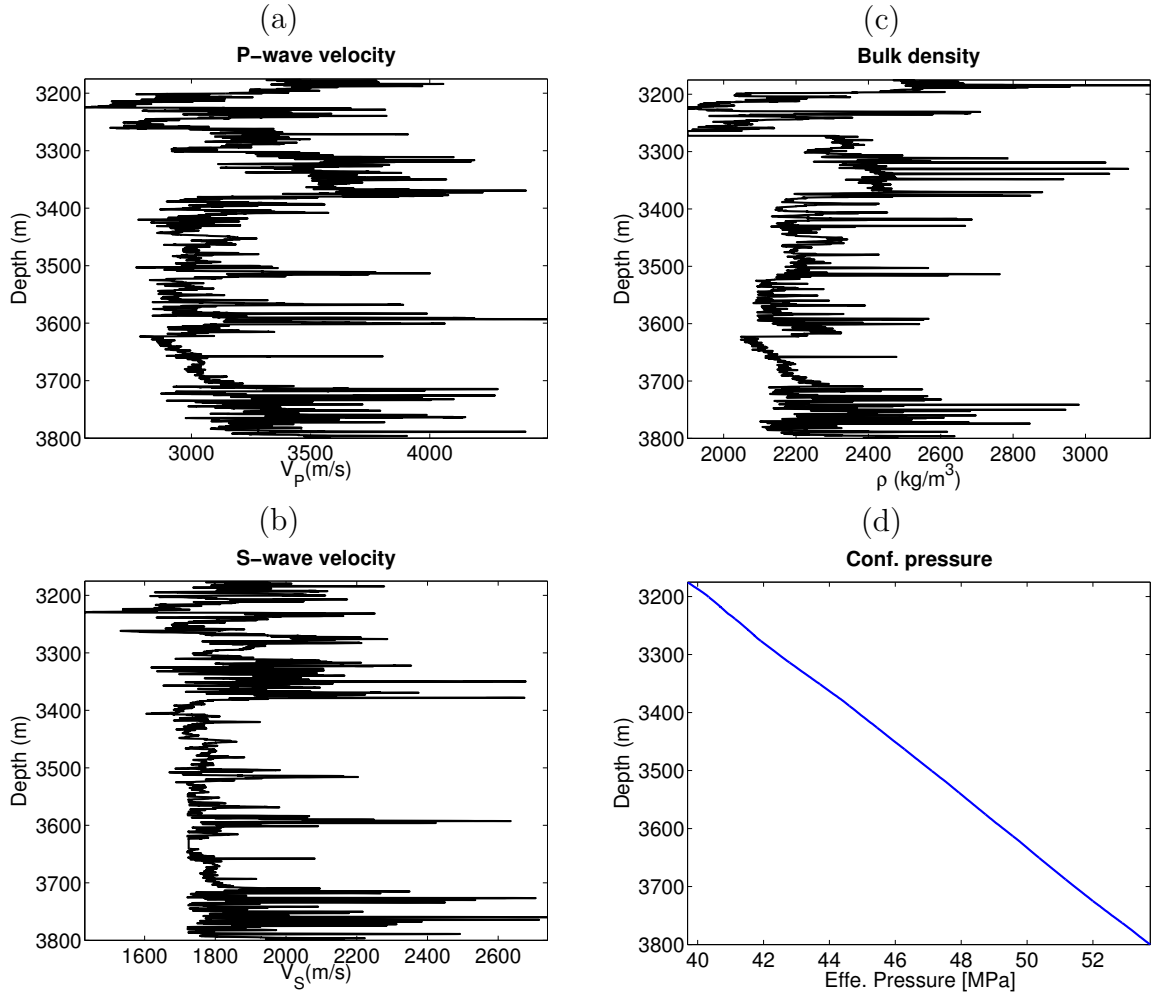
Source: From author

4.1.3 Dynamic similitude (from dynamic stress)

In the case of isotropic media, the stiffness coefficient associated to P-wave propagation is given by,

$$C_{11} = C_{22} = C_{33} = \rho V_P^2 = K + \frac{4}{3}\mu \tag{4.14}$$

In this way, equation (2.18) for dynamic P-wave similitude can be written as follows

$$\Sigma_d^P = \frac{C_{11}^{(f)}}{C_{11}^{(m)}} \frac{\Xi_\nu^P}{\Xi_V^P} = \frac{\rho^{(f)} V_P^{(f)2}}{\rho^{(m)} V_P^{(m)2}} = \frac{(K + \frac{4}{3}\mu)^{(f)}}{(K + \frac{4}{3}\mu)^{(m)}} \tag{4.15}$$

For S-wave, the stiffness coefficient is given by

$$C_{44} = C_{55} = C_{66} = \rho V_S^2 = \mu. \tag{4.16}$$

and consequently, the dynamic S-wave similitude is written as

$$\Sigma_d^S = \frac{C_{44}^{(f)}}{C_{44}^{(m)}} \frac{\Xi_\nu^S}{\Xi_V^S} = \frac{\rho^{(f)} V_S^{(f)2}}{\rho^{(m)} V_S^{(m)2}} = \frac{\mu^{(f)}}{\mu^{(m)}} \qquad (4.17)$$

For mixed P- and S- wave modes

$$C_{12} = C_{13} = C_{23} = C_{11} - 2C_{44} = \rho(V_P^2 - 2V_S^2) = \lambda. \qquad (4.18)$$

In equations (4.15) and (4.17) there is a product of two parameters, i.e., there are several possibilities of densities and velocities in the context of sedimentary rocks that can yield the same value of C_{11} and C_{44}. In other words, $\Sigma_d^P \to 1$ or $\Sigma_d^S \to 1$ does not mean that model and field properties are similar.

For $\Sigma_d^S \to 1$ and $\Sigma_d^S \to 1$, there is the following equation system

$$\rho^{(f)} V_P^{(f)2} = \rho^{(m)} V_P^{(m)2}, \qquad (4.19)$$

$$\rho^{(f)} V_S^{(f)2} = \rho^{(m)} V_S^{(m)2}. \qquad (4.20)$$

To demonstrate that the system of equations above correspond to a non-unicity problem, it is considered the well-log datasets depicted in Figure 4.2. Using the P- and S-wave velocities as well as the density logs, the evaluation of Lamé parameters can be calculated using equations (4.14), (4.16) and (4.18). The elastic stiffness logs are shown in Figure 4.3. The reservoir lies on depths between 3600 and 3700 m, and the rock reservoir is in mainly composed by sandstone (STATOIL, 2001).

Using density (SCHÖN, 2011) and velocity (BOURBIÉ; COUSSY; ZINSZNER, 1987) interval values for sedimentary rocks, all possible values for C_{kl} (including values for P- and S-wave modules) are calculated. These values are depicted in Figure 4.4a. Considering that the mean values of stiffness coefficients $K + \frac{4}{3}\mu$, μ and λ in reservoir interval depth are 20.45, 6.45 and 5.12 MPa, respectively (see Figure 4.3), these corresponding values are separated in the complete C_{kl} matrix. As it is possible to see in Figures 4.4b, 4.4c and 4.4d, fixing velocity values (or the inverse, i.e. fixing density values) gives several density values (or several velocity values) which can provide similar stiffness coefficients values.

4.1.4 Theoretical analysis of dynamic similitude

Supposing that dynamic similitude in context of dynamic stress is a non-unicity problem and proving that a high dynamic similitude does not mean a high similitude of density and velocities, as it was seen in the previous subsection, it is possible to infer that there are factors that better regularize the dynamic similitude. In this subsection the effects of porosity and clay content in the dynamic similitude context are showed.

Figure 4.3 – Lamè's parameters as a function of depth for well 660810-B-4AH from Norne field-Norway. (a) $K + \frac{4}{3}\mu$, (b) μ and (c) λ estimated from P-wave velocity, S-wave velocity and density well-logs depicted in Figure 4.2.
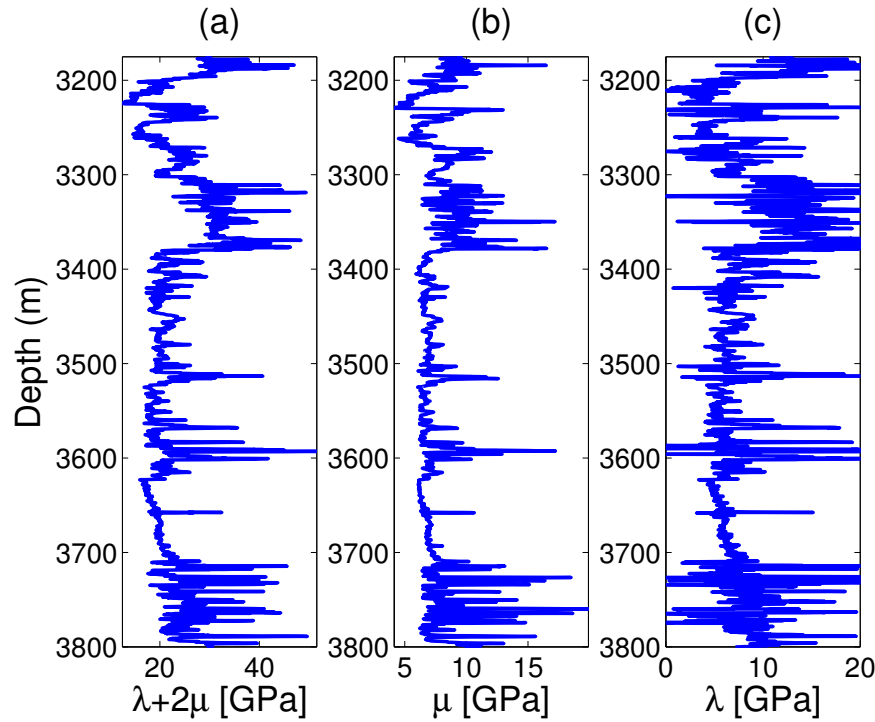
Source: From author.

Table 4.1 – Velocities and density values of different sandstones formations in the subsurface of earth.

Type of natural rock	Dry Vel. V_P (m/s)	Dry Vel. V_S (m/s)	Bulk Density ρ (kg/m^3)	Effective Pressure (MPa)	Clay content (%)	Porosity (%)
Navajo Sandstone (COYNER, 1984)	4200	2800	2316	0	0	11.8
Weber Sandstone (COYNER, 1984)	≈2900	≈2150	2392	10	0	9.5
Sandstone (Sample2) (KOWALLIS; JONES; WANG, 1984)	2520	1610	1860	10.2	6	29.2
Bandera Sandstone* (MANN; FATT, 1960)	2837	1782	2160	10	****	20
Sandstone ♯22 (HAN, 1986)	4030	2400	2280	40	4	20.72
Sandstone ♯24 (HAN, 1986)	4690	2940	2570	40	8	9.12

∗ Information about the clay content is not specified in the paper.

Source: From author.

Figure 4.4 – (a) All possible values of stiffness coefficients for sedimentary rocks. Corresponding isocurves of mean values of (b) K and (c) μ from well 660810-B-4AH of Norne field-Norway.

(a)

(b)

(c)
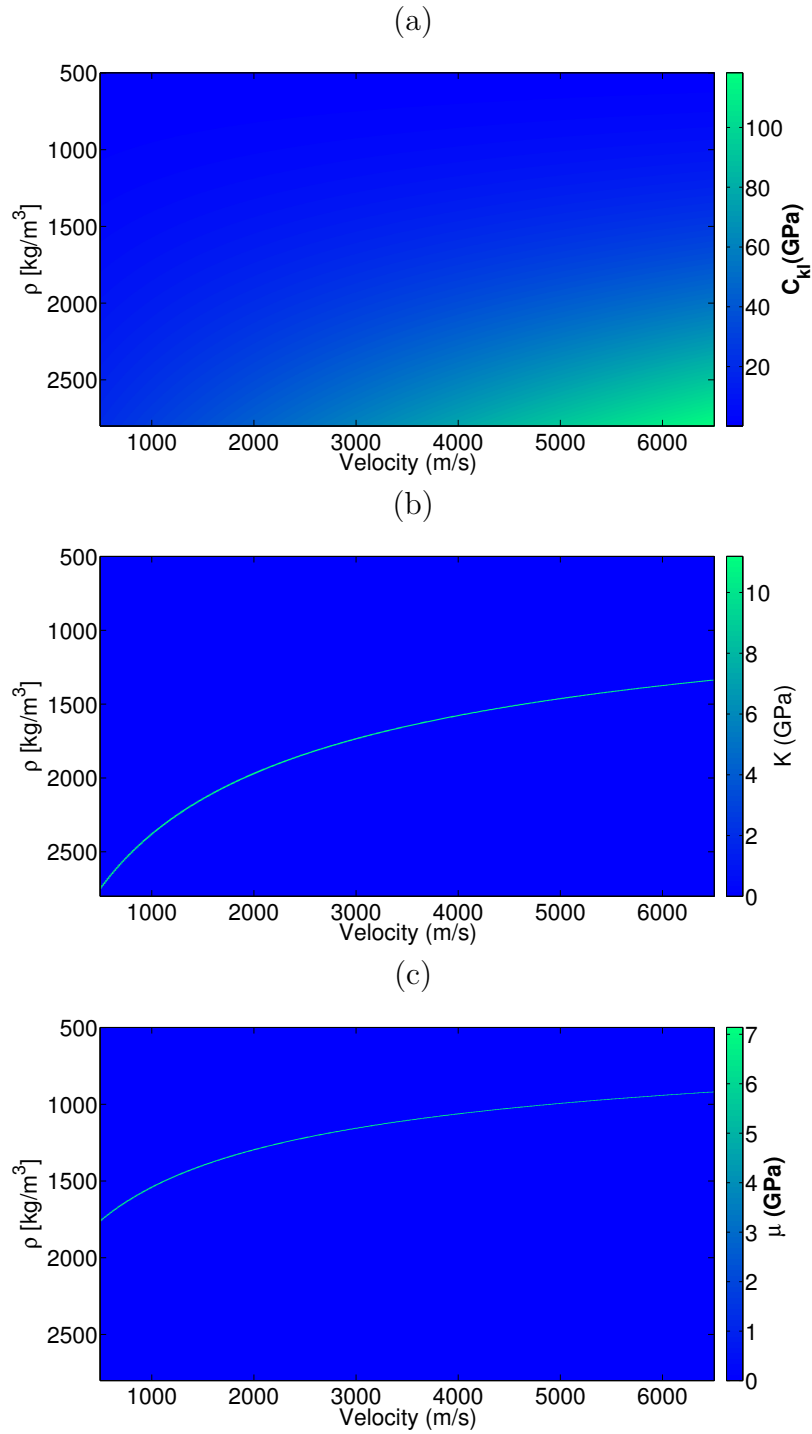
Source: From author.

The relation between density and porosity (SERRA, 2008) as well as the P-wave velocity and porosity (WYLLIE; GREGORY; GARDNER, 1956) in case of clean sandstones is given by

$$\rho_{rock} = (1 - \phi)\rho_{min} + \phi\rho_{fl}, \tag{4.21}$$

or

$$\rho_{rock} = \rho_{min} + \phi(\rho_{fl} - \rho_{min}), \tag{4.22}$$

and

$$\frac{1}{V_{rock}} = \frac{\phi}{V_{fl}} + \frac{1 - \phi}{V_{min}}, \tag{4.23}$$

or

$$V_{rock} = \frac{V_f V_{min}}{\phi V_{min} + (1 - \phi)V_f}. \tag{4.24}$$

where 'fl' stands for fluid and 'min' for mineral or matrix. In the case of sandstones with a given content of clay in its composition the density is given by (SERRA, 2008)

$$\rho_{rock} = \rho_{min}(1 - \phi - V_{sh}) + \rho_{fl}\phi + \rho_{sh}V_{sh} \tag{4.25}$$

where 'fl' stands for fluid, 'min' for mineral or matrix and 'sh' for clay.

For clean sandstone with porosity lower than 37 %, another equation that relates velocity with porosity is the Raymer, Hunt e Gardner ()'s formulation, which mathematically is given by,

$$V_{rock} = (1 - \phi)^2 V_{min} + \phi V_{fl}. \tag{4.26}$$

In equations (4.22), (4.24) and (4.26), the rock density is linear dependent of porosity, while velocity has a non-linear dependence of porosity. Moreover, other empirical equations relating compressional and/or shear velocity with porosity in case of clean sandstones is the Han, Nur e Morgan (1986)s' equation give by

$$V_P = 5020 - 5630\phi \qquad (m/s), \tag{4.27}$$

$$V_S = 3030 - 3780\phi \qquad (m/s), \tag{4.28}$$

where porosity(ϕ) range from 0 to 1. Together with the previous empirical relations, Han, Nur e Morgan (1986) proposed relations of compressional and shear wave velocities in the case of sandstones with a certain amount of clay in their composition. They are given by

$$V_P = 5590 - 6930\phi - 2180V_{sh} \qquad (m/s), \tag{4.29}$$

$$V_S = 3520 - 4910\phi - 1890V_{sh} \qquad (m/s), \tag{4.30}$$

where V_{sh} is the clay content in the rock.

Figure 4.5a shows the density rock as a function of porosity for a sandstone rock type (with quartz as its main mineral). For porosity range from 0 to 100 % the density

interval varies from 2546 (density of quartz mineral) to 0 (air density) kg/m^3. As it is depicted in Figure 4.5a, the porosity value in the graph is that one from Navajo Sandstone (COYNER, 1984) ($\phi = 11.8\%$). In Figure 4.5a the density correspondent to 11.8 % is 2246 kg/m^3. This density value is very similar to the one of Navajo Sandstone (COYNER, 1984) ($\rho = 2316\ kg/m^3$). Based on this comparison, the ratio between the Navajo Sandstone density and the density found in the curve built based on the equation (4.21) is 1.02, i.e., nearly 1. In this approximation it was disregarded any contamination by clay and the fluid density (air) was considered zero. Figure 4.5b shows the estimative of P-wave velocity (bulk) versus porosity for a clean sandstone based on equations (4.24) and (4.26). As it is shown in Table (4.1), e. g., the P-wave velocity of Navajo Sandstone (COYNER, 1984) is 4200 m/s, while the velocity predicted by Wyllie, Gregory e Gardner (1956) and Raymer, Hunt e Gardner ()'s equations were, respectively, 4319 m/s and 1971 m/s, respectively. The velocity values for simulated sandstones considered the velocity values range from 5500 m/s (velocity in quartz) to $\approx 340\ m/s$ (air velocity). Figure 4.5c shows the estimative of P and S-wave velocities (bulk) versus porosity for a clean sandstone based on equations (4.27) and (4.28). For porosity of 11.8 % the correspondent velocity values are 4356 m/s (for P-wave) and 2600 m/s (for S-wave). For this situation, the ratio between the Navajo Sandstone velocities (P and S) and the velocities of a synthetic sandstone sample built based on equations (4.27) and (4.28) are 0.96 (P-wave) and 1.07 (S-wave). The result of Vp ratio found using equation (4.27) was the best among the equations used in this procedure.

In the next step, it was analyzed the influence of clay content in density and velocities in dynamic similitude. First, the density curves were estimated based on the equation 4.25. The density curves are generated for values of porosity and clay content raging from 0 to 100%. From the porosity and clay content corresponding to values of sample 22 the density was 2282 kg/m^3, while for sample 24 the value was 2448 kg/m^3. The ratios between the real (see Table 4.1) values of density from samples 22 and 24 and the values from the curves depicted in Figure 4.6 are, respectively, 0.99 and 1.04. This high similitude in the estimated density shows that equation equation 4.25 is feasible constraining for bulk density in shaley sand samples.

Second, the similitudes for P and S-wave velocities were investigated. Figures 4.7a and 4.7b show the estimatives of P and S-wave velocities (bulk) versus porosity based on equations (4.29) and (4.30). Again the samples 22 and 24 from (HAN; NUR; MORGAN, 1986) were taken into account as reference samples. The velocities estimated for sample 22 corresponding to porosity of 20.72% and a clay content of 4% (see Table 4.1) were 4067 m/s and 2427 m/s. Consequently, the P- and S-wave velocity ratios between the real velocities for sample 22 (see Table 4.1) were 0.99 and 0.98, respectively. The curves of Figure 4.7b were generated also using the equations using the equations (4.29) and (4.30). However, the analysis now relies on sample 24. The P- and S-wave velocities estimated for

Figure 4.5 – (a) Estimative of rock sandstone density based on equation (4.21). The red dot indicates the density value correspondent to the porosity of Navajo Sandstone. (b) Estimative of P-wave velocity (bulk) based on equations (4.24) and (4.26). (c) Estimative of P- and S-wave velocities (bulk) based on the equations (4.27) and (4.28)

(a)

(b)

(c)
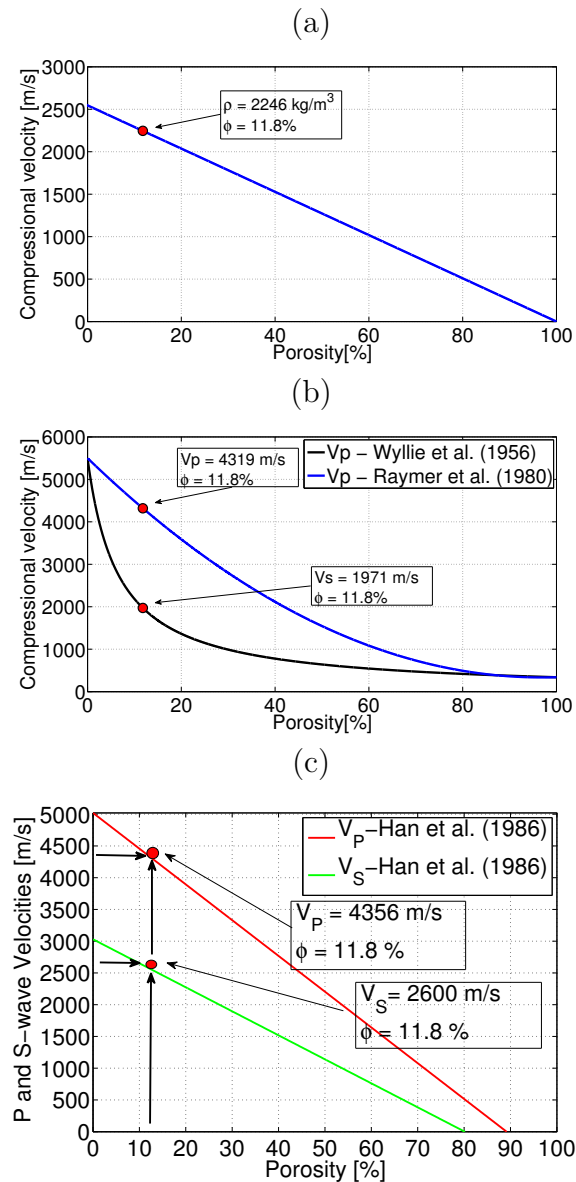
Source: From author

porosity of 9.12% and clay content of 8% were 4784m/s and 2912m/s, respectively. The P- and S-wave velocity ratios between the real values of sample 24 depicted at Table 4.1 and the estimated values by equations (4.29) and (4.30) were 0.98 and 1.009, respectively. Using the ratios of density, P- and S-wave velocities, the dynamic similitudes for P- and S-waves were calculated for samples 22 and 24. The dynamic similitudes for P-wave were 0.98 (sample 22) and 1.009 (sample 24). In the case of similitude for S-wave for both samples the values were 0.97 and 1.07, respectivelly.

The estimative of rock density and velocity in Figures 4.5, 4.7 and 4.6 shows that equations equation 4.21, (4.29) and (4.30) important constraints to reproduce a desirable geological structure in laboratory, with a good agreement between the velocities and densities, and a good dynamic similitude as well. As It was shown above, the dynamic similitude values estimated from the curves based on empirical relations showed an error lower than 1 %, that proves this good agreement and importance in controlling these two factors. The question that arises is how to control in laboratory these two parameters in order to obtain the elastic parameter similar to any geological structure, which is desire to simulate. In the next section, it is showed that this task is not easy to be performed. However, these constrains were tested in different scenarios and comparison between real rocks and synthetic rocks were performed.

4.2 Experimental results

In this section, some curves will be generated in order to experimentally analyze the dynamic similitude equations in Chapter 2. It will be generated curves of P-wave, S-wave, density and porosity ratios, as well as curves of P- and S-wave dynamic similitudes.

4.2.1 Influence of mineralogical composition in physical properties

The influence of mineralogic composition of the samples in their properties is analyzed, specially the influence of cement and clay content. Figures 4.8, 4.9 and 4.10 show the variation of velocities, density and porosity with varying concentration of cement for samples AA, 3A and E, respectively. Figure 4.8 shows the curves for samples AA. As said before, these samples have the same composition as samples 3A, but were constructed with a different methodology. While the velocity curves for samples 3A show a clear increase in velocities with cement concentration and a decrease in porosity, which is a pertinent behavior when increasing cement concentration, the second shows an increase in velocities until a certain point. After this point the velocities begin decreasing, showing the lowest values for the highest cement concentration. This trend is followed by density curve. Porosity curves also show this unexpected behavior, presenting the highest porosity value

Figure 4.6 – Estimative of density based on equations 4.25. (a) The red dot indicates the correspondent density value estimated to porosity and clay content of sample 22 and (b) for sample 24 .

(a)

(b)
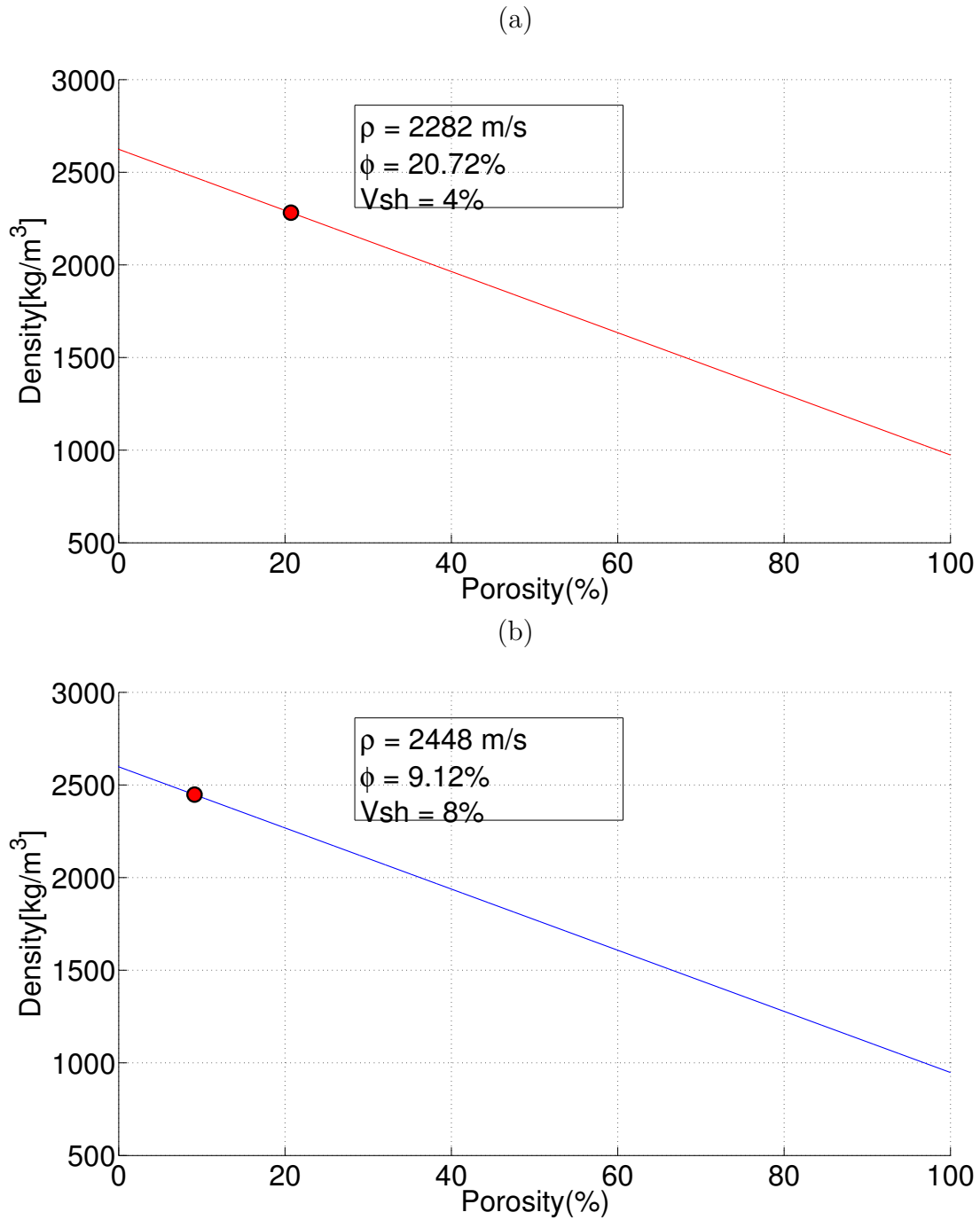
Source: From author

Figure 4.7 – Estimative of P-wave velocity (bulk) based on equations 4.29 and 4.30. The red and blue dots indicate the P- and S-wave velocities estimated based on the porosity and clay content of samples (a) 22 and (b) 24.

(a)

(b)
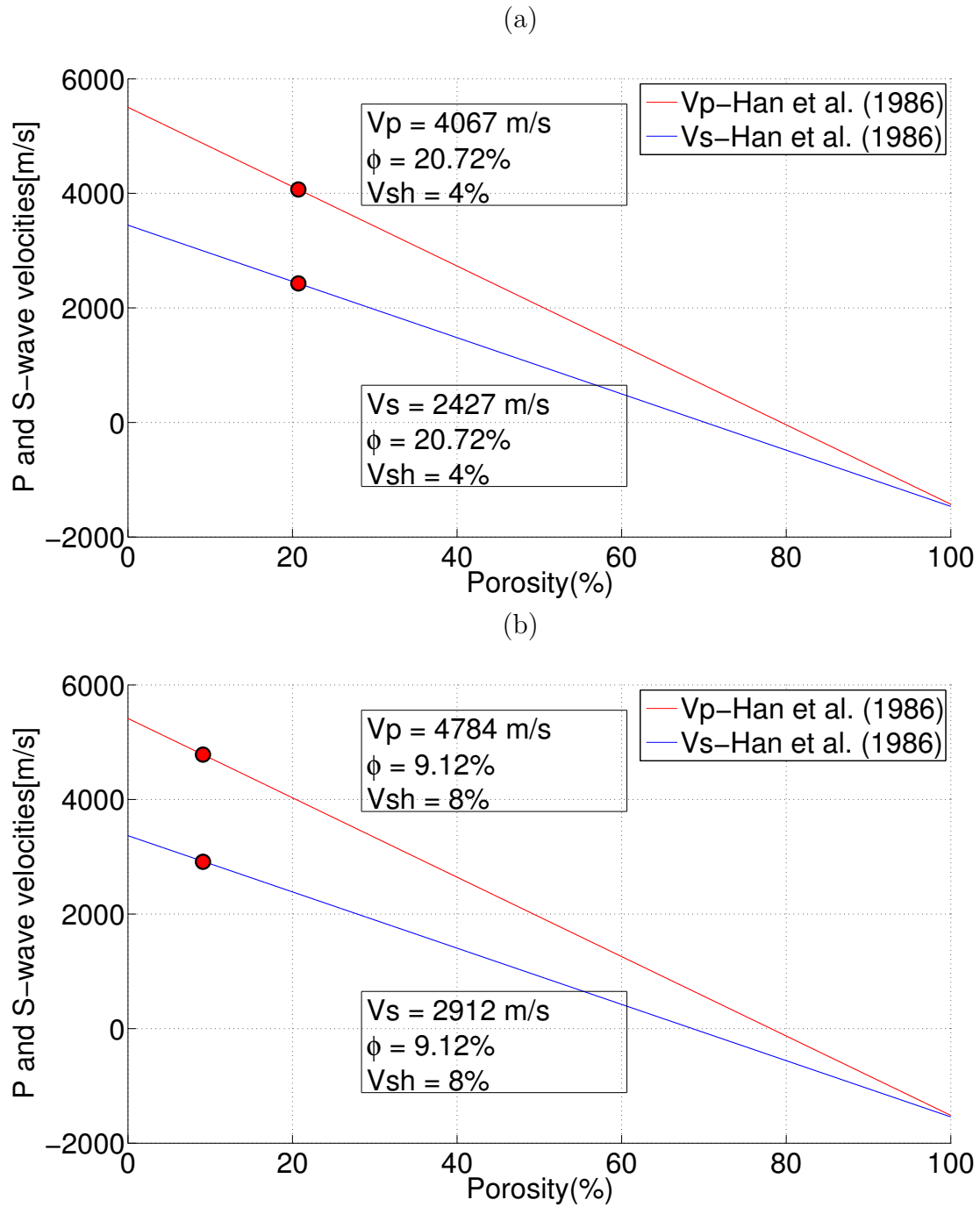
Source: From author

for the highest cement concentration. These uncommon patterns are probably caused by the loss of material that happened in the construction of these samples. Most of material lost was cement, that is finer than sand. The samples with higher concentration of cement suffered higher loss, that is why their values are very far from the expected response.
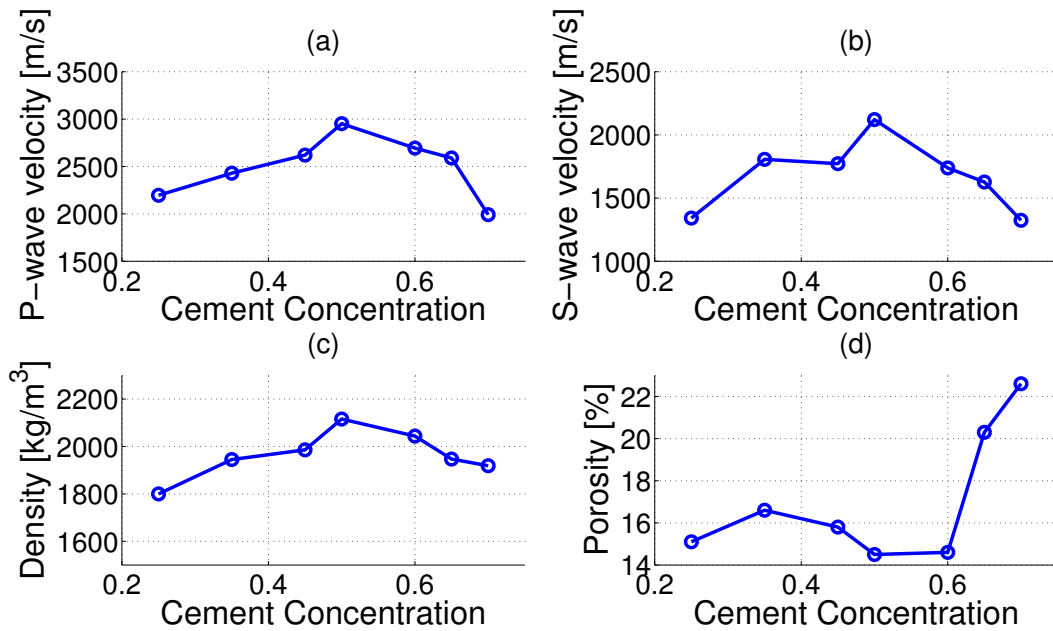
Figure 4.8 – Elastic and petrophysical properties of group AA samples. a) P-wave velocity, b) S-wave velocity, c) density and d) porosity variation with increasing cement concentration.

Source: From author

For other group of cemented sandstones without clay (see Figure 4.9) it is visible a high increase in velocities with the increasing of cement concentration. There is a smooth decrease between 50% and 60%, which could have been caused by small error in the applied pressure. The density curve follows the same trend as velocities. On the other side, the porosity values rapidly decreased as the cement concentration increased, an expected behavior if compared with velocities and density curves. This trend is probably caused by the fact that cement occupies the pores of the rock, causing a very low value of porosity for a high cement concentration.

Figure 4.10 shows the curves of the group E samples. The curves of velocity have the same trend as the curves of Figure 4.9, with an increase with increasing cement concentration. However, the overall velocity values are lower that the values for samples 3A. This behavior is probably caused by the fact that clay is present in the composition of these samples, which decreases their velocities, along with a small concentration of cement. The density of 10% for cement concentration was higher than the same value for samples 3A. This can be an indicative that the presence of clay in the samples highly increase their densities. The porosity values for cement concentration of 10% and 15% are lower than the values for samples 3A. This happens because, in the absence of a high amount of

Figure 4.9 – Elastic and petrophysical properties of group 3A samples. a) P-wave velocity, b) S-wave velocity, c) density and d) porosity variation with increasing cement concentration.
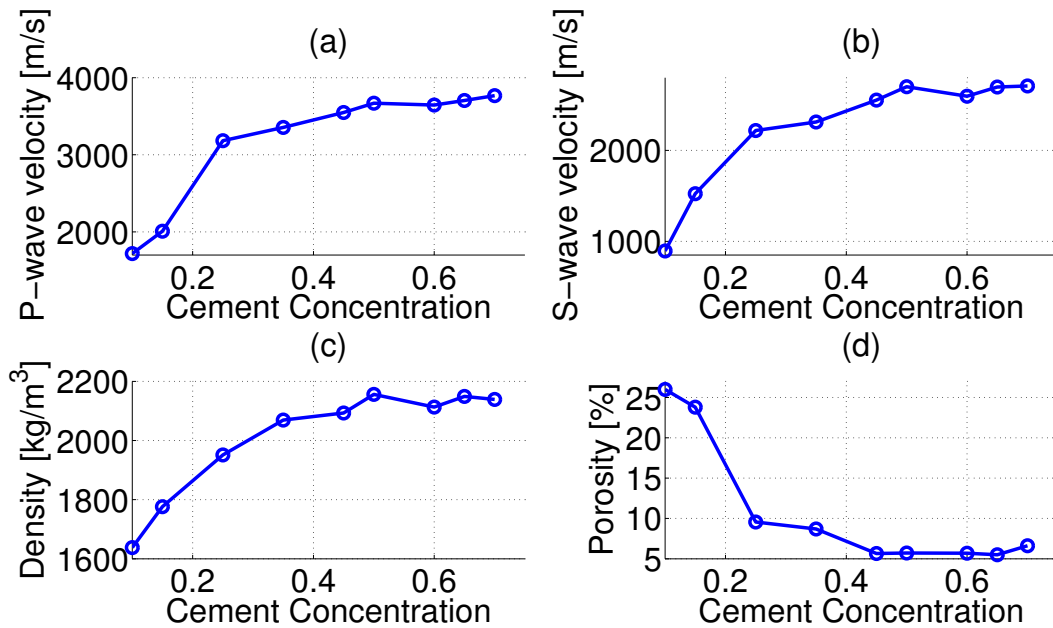

Source: From author

cement, clay fills the pores of the synthetic rock, decrease the porosity values. The other values of porosity have close values, which is explained by the small variation in cement and clay content. If there is a decrease in cement concentration, there is an increase in clay content that keeps the pores filled in a similar fashion.

These analyses are very important to observe the influence of materials used in the preparation of samples in their elastic and petrophysical characteristics. It is clear that the cement has a very important role in the velocity of synthetic rocks. Because the high velocity of this material itself, as described in Table 3.4, its presence rapidly increase the velocity of the samples. Also, because of the size of cement grains, this material occupies the pores of sandstones when mixture with sand. The high presence of cement rapidly decreases the porosity of samples. On the other side, the presence of clay decreases the velocity of samples, even with a low concentration of the material, and increases the density. Furthermore, the analyses were very important to help to design the optimal process of fabrication of the samples. It was proved that high loss of material influence in the properties of samples.

4.2.2 Dynamic similitude analysis for synthetic sandstones

Proceeding with the experimental analysis of the non-unicity problem in the dynamic similitude, the elastic properties of Bandera Sandstone (MANN; FATT, 1960) were chosen to be compared with properties of samples AA, depicted in Table 3.4. Figure

Figure 4.10 – Elastic and petrophysical properties of group E samples. a) P-wave velocity, b) S-wave velocity, c) density and d) porosity variation with increasing cement concentration.
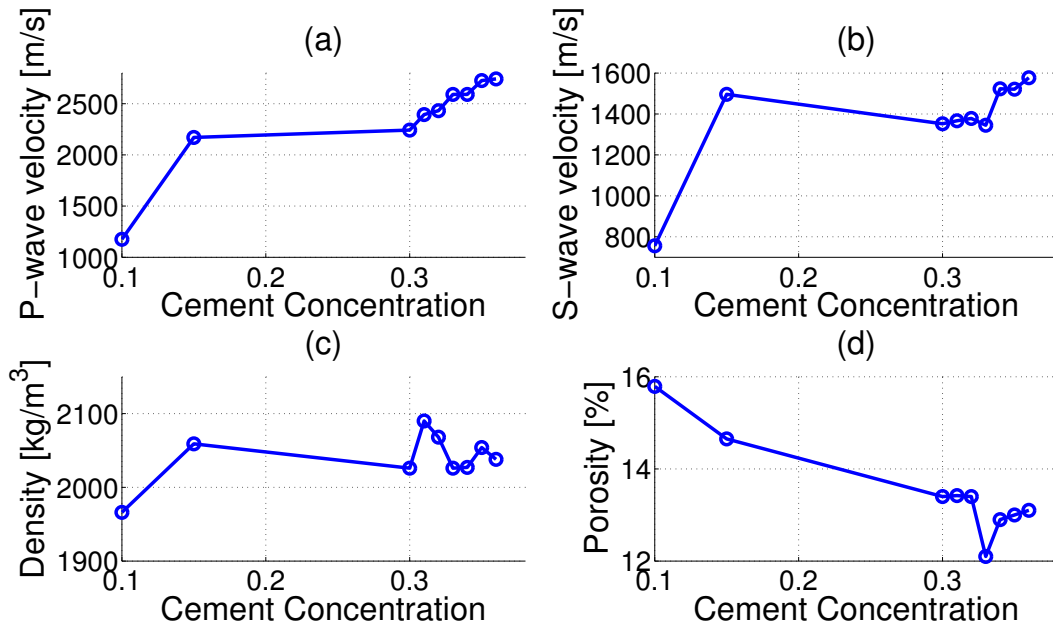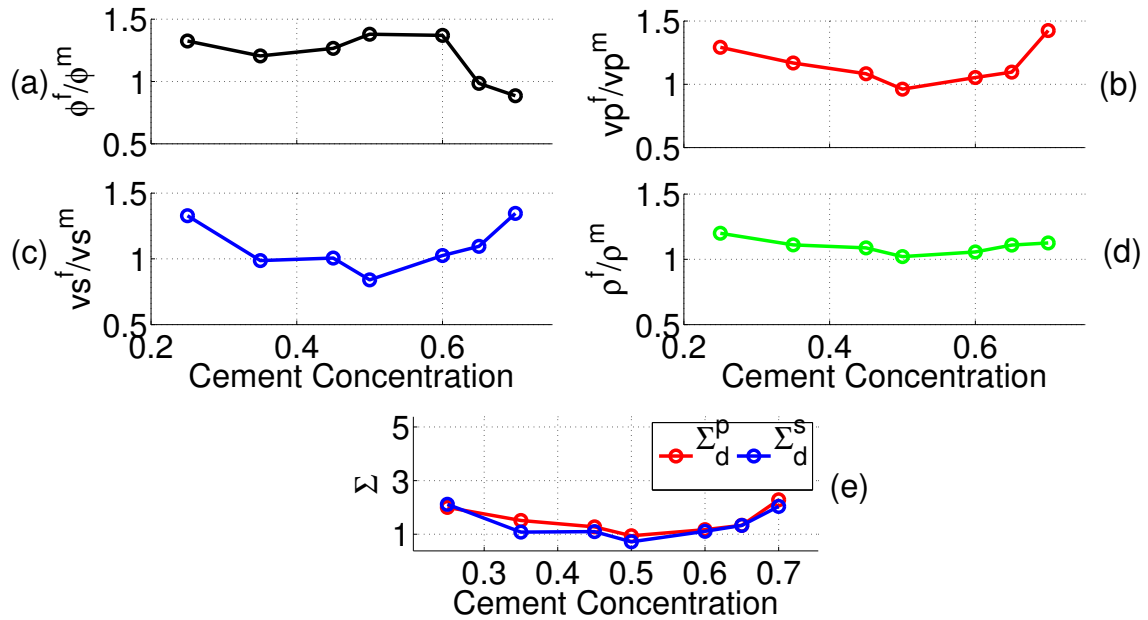

Source: From author

4.11e depicts the P and S-waves dynamic similitudes for all the samples. The best dynamic similitude for P-wave is related to cement concentration of 50% (0.94). In Figure 4.11b it is possible to see the P-wave velocity ratio is the best for this concentration. The same is found for density ratio. However, for the best S-wave Dynamic similitude, whose best result is for concentration 0.35% (1.08), the associated density ratio is far from 1 (1.11). In other words, the analyses made in these curves showed that the best dynamic similitude (i.e. approximately 1) may not indicate good fits of density or velocities ratios. For this case, it is possible to argument that an optimum dynamic similitude does not means that all the properties of field and model are similar.

The second comparison was made between samples 3A and Weber Sandstone (COYNER, 1984). The curves depicted in Figure 4.12 clearly show the best similarity in porosity for 25% and 35% of cement (0.99 and 1.09). The P and S-waves ratios for 25% of cement concentration are 0.91 and 0.96 and for 35% of cement concentration are 0.86 and 0.92. However, for these two concentrations the density ratios are quite different (the ratios are 1.22 and 1.15). The densities of the synthetic rocks were under estimated, since the ratios of density in both cases (25% and 35%) are higher than 1. Using these ratios, the dynamic similitudes were estimated and their respective values are shown in Figure 4.12e. For 25 % and 35 % of cement concentration, the dynamic similitude similitude for P- and S-wave are: (Σ_P=1.01, Σ_S=1.15) and (Σ_P=0.86, Σ_S=0.99). It is worthy to mention that the mineralogy of the Weber Sandstone (COYNER, 1984) is not completely known. This can be the cause of the distance from 1 of both dynamic similitudes and

Figure 4.11 – Comparison between elastic and petrophysics properties of Bandera Sandstone and synthetics samples AA . The graphics show: a) the porosity ratio, b) the P-wave velocity ratio, c) the S-wave velocity ratio, d) the density ratio and e) the dynamic similitudes

Source: From author

density ratios.

The third comparison of similitudes is made for sandstones with clay. The comparison is performed between samples E and 2-sandstone sample extracted from (KOWALLIS; JONES; WANG, 1984). This rock is a sandstone with 6 % of clay in its composition, but its entire mineralogical composition is not described. Since the values of porosity in these samples are almost all similar (ranging from 12% to 15%), the similarity of clay content is analyzed as the key factor for a good dynamic similarity. Figures 4.13b and c show that the P and S-waves ratios for 34% of cement concentration (that correspond to 6 % of clay) are 0.95 and 1.06. As can be seen in Figure 4.13d, the density ratio ranges from 0.89 to 0.94 and, for cement concentration of 34%, the density ratio is 0.91. It is worthy to mention that the highest ratio of density does not correspond to the highest ratio in V_P and V_S. For 34% of cement concentration, the dynamic similitudes for P- and S-waves are: $(\Sigma_P = 0.86, \Sigma_S = 1.02)$. Taking into consideration the two dynamic similitudes, the best result is for cement concentration of 34%, if compared to the other concentrations. This result shows that the best ratio of clay content may give the best dynamic similitudes results. If the total mineralogy of the real rock was known, the result probably would be way better.

Figure 4.12 – Comparison between elastic and petrophysics properties of Weber Sandstone and synthetics samples 3A . The graphics show: a) the porosity ratio, b) the P-wave velocity ratio, c) the S-wave velocity ratio, d) the density ratio and e) the dynamic similitudes.
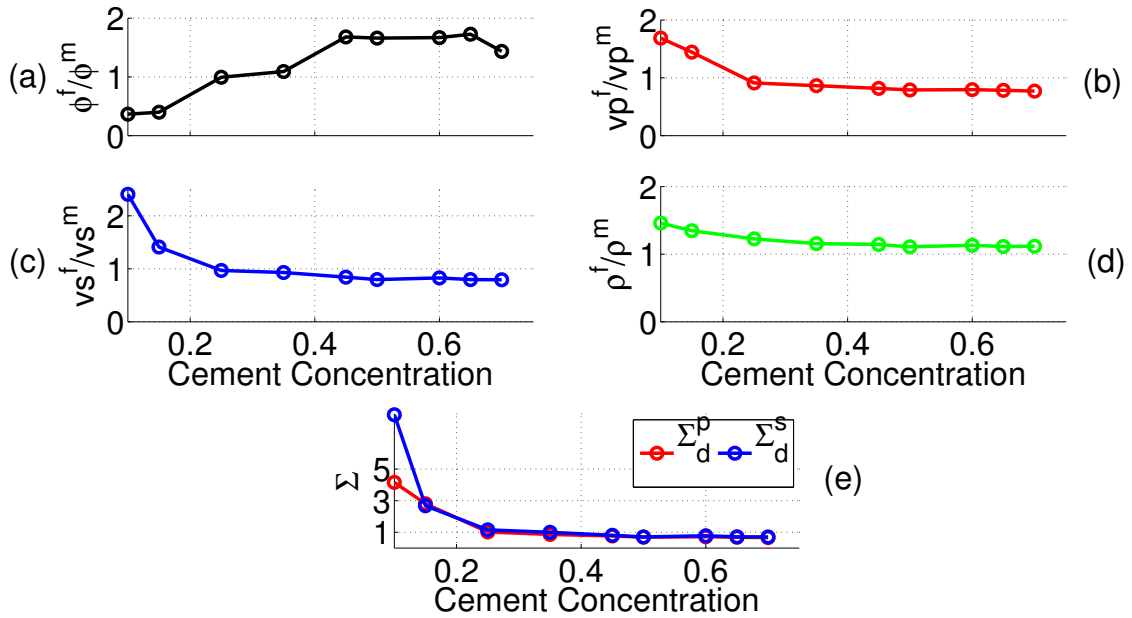

Source: From author

Figure 4.13 – Comparison between elastic and petrophysics properties of sample 2-sandstone from and samples E. The graphics show: a) the porosity ratio, b) the P-wave velocity ratio, c) the S-wave velocity ratio, d) the density ratio and e) the dynamic similitudes.
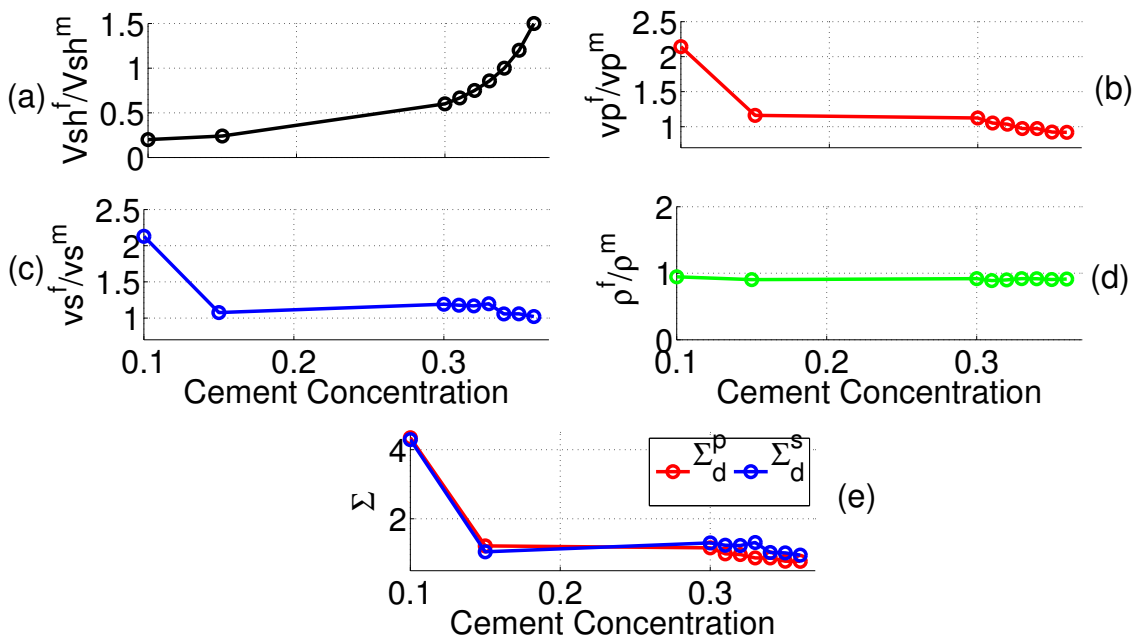

Source: From author

4.3   Final considerations

Previously, it was described that for a given mineralogy, controlling the effective pressure, porosity and clay content on a synthetic rock, it is possible to achieve high similitudes between real and synthetics rocks. In this procedure, some observations may have to be considered. First of all, it is very difficult to find all information about velocity, density, porosity, clay content, effective pressure and mineralogy of a rock in general literature. So in most of times, the real samples used in this process that have their properties compared to synthetic rocks are considered as dry sandstones, with or without a given amount of clay in their composition. Consequently, a more detailed information about the rock mineralogy is missing . These uncertain information may be prejudicial to the analysis of similitude, being one of the constraints that must be taking into account in future works.

Second, as long as cement is used as a composition of all the samples, in order to get the samples hard, its effect on the properties of the samples must be considered. In a synthetic sandstone, the high concentration of cement may cause uncommon values of velocity, density and porosity. For example, if a synthetic sandstone has a cement concentration of 70%, their properties become very distant from the properties of real sandstones. Comparing these kind of rock with real sandstones is not reliable, probably giving wrong results. In other words, sandstones samples with high concentration of cement have their mineralogical composition very distant from the composition of real sandstones.

Finally, as depicted in Figures 4.11e, 4.12e and Figure 4.13e, a good dynamic similitude can be achieved in laboratory, even if the mineralogical composition of real rock is not totally known. Obviously, these results would be better if the total mineralogies were reproduced. Also, from the curves generated in both comparisons, it can be seen that the porosity and clay content are parameters that regularize the dynamic similitude.

5 CONCLUSIONS

In this work, a mathematical analysis of physical similitudes in context of experimental seismic modeling is performed. The three physical similitudes were investigated in order to compare the similitude between a real rock formation and a synthetic seismic medium manufactured at laboratory. On the basis of our analysis, the following observations can be made:

1) The geometrical and kinematic similitude are almost always reached in laboratory environment, due to the geometrical features of geological layers that can be reproduced at laboratory and to 'some' types of material that have the same velocity of a geological layer of interest.

2) The use of kinematic similitude provided a clear demonstration of upscale of frequency from field to laboratory. According to the necessity and the type of media desired to simulate, the affordable source frequency should be chosen in order to better acquire a signal with better quality.

3) Using the approximation of plane-wave solution of wave propagation in isotropic media, it was showed that the dynamic similitude (in context of dynamic stress) depends on elastic impedance or elastic stiffness coefficients.

4) According to our analysis, the dynamic similitude (in context of dynamic stress) is an non-unicity problem. The physical consequences of this ambiguity is a remarkable feature, namely, the fact that different density with different velocity values around the exact value may present the same elastic stiffness coefficients.

5) The porosity control is a preponderant constraint in order to reach a suitable similitude between real and manufactured synthetic rocks on a dynamic stress point of view. Other priori informations (by using empirical equation), such as formation temperature, clay volume content, secondary porosity and effective pressure formation can be used in the regularization of this non-unicity problem.

6) The non-unicity problem and the fact that porosity and clay content may regularize the dynamic similitudes are experimentally proved by the use of synthetic samples constructed in this laboratory.

Moreover, some other remarks can be made in order to enhance the quality of the analyses realized in this work. One important thing that can be realized in future works is compare the dynamic similitudes for a larger number of real rocks, in order to enhance the reliability of this analysis, for a larger number of comparisons. Another crucial thing to be realized is to find a more reliable way to reproduce other synthetic sandstones in laboratory

using different method of construction. The use of cement provided good results, but the results could have been better and more reliable if the samples had a mineralogical composition closer to real sandstones. This procedure is possible if ideal conditions of pressure and temperature are achieved in laboratory. Also, to get more information about mineralogy of real sandstones is another constraint that could be enhanced.

BIBLIOGRAPHY

ALHUSSAIN, M.; GUREVICH, B.; UROSEVIC, M. Experimental verification of spherical-wave effect on the AVO response and implications for three-term inversion. *Geophysics*, v. 73, n. 2, p. C7–C12, 2008.

ASSAD, J. M. et al. Elastic wave propagation in a medium containing oriented inclusions with a changing aspect ratio: A physical model study. *Geophysical journal international*, v. 125, n. 1, p. 163–172, abr. 1996.

ASSAD, J. M. et al. A physical model study of scattering of waves by aligned cracks: Comparison between experiment and theory1. *Geophysical prospecting*, v. 41, n. 3, p. 323–339, abr. 1993.

BARRIÈRE, J. et al. Laboratory monitoring of P waves in partially saturated sand. *Geophysical journal international*, v. 191, n. 3, p. 1152–1170, 2012.

BOURBIÉ, T.; COUSSY, O.; ZINSZNER, B. *Acoustics of Porous Media*. [S.l.]: Gulf Publishing Company, Book Division, 1987.

BUCKINGHAM, E. On physically similar systems; illustrations of the use of dimensional equations. *Physics review*, v. 4, p. 345–376, 1914.

CARCIONE, J. et al. Pore pressure estimation in reservoir rocks from seismic reflection data. *Geophysics*, v. 68, n. 5, p. 1569–1579, set. 2003.

CARCIONE, J. M.; HERMAN, G. C.; KROODE, A. P. E. ten. Seismic modeling. *Geophysics*, v. 67, n. 4, p. 1304–1325, 2002.

CARTER, h.; PAMBAYUNING, S. Extended bandwidth by a frequency domain merge of two 3d seismic volumes. *The leading edge*, v. 28, n. 4, p. 400–406, 2009.

CHEADLE, S. P.; BROWN, R. J.; LAWTON, D. C. Orthorhombic anisotropy; a physical seismic modeling study. *Geophysics*, v. 56, n. 10, p. 1603–1613, 1991.

COATES, R. T.; SCHOENBERG, M. Finite-difference modeling of faults and fractures. *Geophysics*, v. 60, p. 1514–1526, 1995.

COYNER, K. B. *Effects of stress, pore pressure, and pore fluids on bulk strain, velocity, and permeability in rocks*. Thesis, 1984.

EBROM, D. A.; MCDONALD, J. A. *Seismic Physical Modeling*. 1st edition. ed. Tulsa, Okla: Society Of Exploration Geophysicists, 1994.

FAR, M. E. et al. Measurements of seismic anisotropy and fracture compliances in synthetic fractured media. *Geophysical journal international*, v. 197, n. 3, p. 1845–1857, 2014.

FIGUEIREDO, J. J. S. de et al. Estimating fracture orientation from elastic-wave propagation: An ultrasonic experimental approach. *Journal of geophysical research: solid earth*, v. 117, n. B8, p. B08304, 2012.

FIGUEIREDO, J. J. S. de et al. Shear wave anisotropy from aligned inclusions: ultrasonic frequency dependence of velocity and attenuation. *Geophysical journal international*, v. 193, n. 1, p. 475–488, 2013.

FRENCH, W. Two dimensional and three dimensional migration of model experiment reflection profiles. *Geophysics*, v. 39, n. 3, p. 265–277, jun. 1974.

FRENCH, W. Computer migration of oblique seismic reflection profiles. *Geophysics*, v. 40, n. 6, p. 961–980, dez. 1975.

HAN. Effects of porosity and clay content on acoustic properties of sandstones and unconsolidated sediments. 1986.

HAN, D.-h.; NUR, A.; MORGAN, D. Effects of porosity and clay content on wave velocities in sandstones. *Geophysics*, v. 51, n. 11, p. 2093–2107, 1986.

HEARN, S.; HENDRICK, N. Bandwidth requirements for shallow, high-resolution seismic reflection. In: *ASEG Extended Abstracts 2001: 15th Geophysical Conference.* [S.l.]: Australian Society of Exploration Geophysicists (ASEG), 2001, (ASEG Extended Abstracts). p. 1–4.

HELLER, V. Scale effects in physical hydraulic engineering models. *Journal of hydraulic research*, v. 49, n. 3, p. 293–306, 2011.

HSU, C.-J.; SCHOENBERG, M. Elastic waves through a simulated fractured medium. *Geophysics*, v. 58, n. 7, p. 964–977, jul. 1993.

HUANG, L.; STEWART, R. R.; DYAUR, N. Elastic properties of 3d-printed rock models: Dry and saturated cracks. In: *AGU Fall Meeting Abstracts.* EUA: [s.n.], 2014. p. 4320.

HUGHES, S. A. *Physical models and laboratory tecnhiques in coastal engineering.* London: World scientific, 1993.

KLINE, J. S. *Similitude and Approximation Theory.* New York: Springer-Verlag, 1986.

KOWALLIS, B. J.; JONES, L. E. A.; WANG, H. F. Velocity-porosity-clay content systematics of poorly consolidated sandstones. *J. geophys. res.*, v. 89, p. 10355–10364, 1984.

MAHMOUDIAN, F. et al. Azimuthal amplitude variation with offset analysis of physical modeling data acquired over an azimuthally anisotropic medium. *Geophysics*, v. 80, n. 1, p. C21–C35, 2015.

MANN, R. L.; FATT, I. Effect of pore fluids on the elastic properties of sandstone. *Geophysics*, v. 25, n. 2, p. 433–444, 1960.

MARGHITU, D. B. *Mechanical Engineer's Handbook.* [S.l.]: Academic Press, 2001.

MARION, D.; MUKERJI, T.; MAVKO, G. Scale effects on velocity dispersion: From ray to effective medium theories in stratified media. *Geophysics*, v. 59, n. 10, p. 1613–1619, 1994.

NAKAGAWA, S.; SCHOENBERG, M. A. Poroelastic modeling of seismic boundary conditions across a fracture. *Journal of the acoustical society of america*, v. 122, p. 831–847, 2007.

OMOBOYA, B. et al. Experimental study of the influence of fluids on seismic azimuthal anisotropy. *Journal of petroleum science and engineering*, v. 130, p. 46–54, 2015.

RATHORE, J. S. et al. P- and S-wave anisotropy of a synthetic sandstone with controlled crack geometry. *Geophysical prospecting*, v. 43, n. 6, p. 711–728, ago. 1995.

RAYMER, L. L.; HUNT, E. R.; GARDNER, J. S. An improved sonic transit time-to-porosity transform. *IN: LOGGING SYMPOSIUM TRANSACTIONS 21st,1980. ANNUAL... Laffayete, Louisiana,* Society of petrophysicist and well-log analyst, 1980, p. 1–13.

SAENGER, E. H. N.; SHAPIRO, S. A. Effective velocities in fractured media: a numerical study using the rotated staggered finite-difference grid. *Geophysical prospecting*, v. 50, p. 183–194, 2002.

SANTOS, L. K. et al. On the source-frequency dependence of fracture-orientation estimates from shear-wave transmission experiments. *Journal of applied geophysics*, v. 114, p. 81–100, 2015.

SCHAKEL, M. D. et al. Seismoelectric interface response: Experimental results and forward model. *Geophysics*, v. 76, n. 4, p. N29–N36, 2011.

SCHÖN, J. H. *Physical properties of rocks: a workbook.* [S.l.]: Elsevier, 2011.

SERRA, O. *Well logging handbook.* [S.l.]: Editions OPHRYS, 2008.

SHERLOCK, D.; MCDONALD, J.; EVANS, B. Seismic imaging of sandbox models. In: *SEG Technical Program Expanded Abstracts 1997.* [S.l.]: Society of Exploration Geophysicists, 1997. (SEG Technical Program Expanded Abstracts), p. 1371–1374.

SHERLOCK, D. H.; EVANS, B. J. The development of seismic reflection sandbox modeling. *AAPG bulletin*, v. 85, n. 9, p. 1645–1659, 2001.

STATOIL. *Norne Field Reservoir Management Plan.* [S.l.], 2001.

STEWART, R. R. et al. Physical modeling of anisotropic domains: Ultrasonic imaging of laser-etched fractures in glass. In: . [S.l.: s.n.], 2011. p. 2865–2869.

SUN, M.; HAN, D.; BATZLE, M. co_2 velocity measurements and models for temperatures down to -10°c and up to 200°c and pressures up to 100 mpa. In: *SEG Technical Program Expanded Abstracts 2009.* [S.l.]: Society of Exploration Geophysicists, 2009, (SEG Technical Program Expanded Abstracts). p. 2090–2094.

TANTSEREVA, A. et al. Numerical modeling of 3d zero-offset laboratory data by a discretized Kirchhoff integral method. *Geophysics*, v. 79, n. 2, p. T77–T90, 2014.

TEODORESCU, P. P. *Mechanical systems, classical models.* [S.l.]: Springer Science & Business Media, 2007. v. 1.

TILLOTSON, P. et al. Observations of fluid-dependent shear-wave splitting in synthetic porous rocks with aligned penny-shaped fractures. *Geophysical prospecting*, v. 59, n. 1, p. 111–119, 2011.

VAVRYUK, V. Real ray tracing in anisotropic viscoelastic media. *Geophysical journal international*, v. 175, p. 617–626, 2008.

VERNIK, L.; NUR, A. Ultrasonic velocity and anisotropy of hydrocarbon source rocks. *Geophysics*, v. 57, n. 5, p. 727–735, 1992.

VIRIEUX, J.; CALANDRA, H.; PLESSIX, R.-É. A review of the spectral, pseudo-spectral, finite-difference and finite-element modelling techniques for geophysical imaging. *Geophysical prospecting*, v. 59, p. 794–813, 2011.

WANG, Z. et al. Experiment study of pore structure effects on velocities in synthetic carbonate rocks. *Geophysics*, v. 80, n. 3, p. D207–D219, 2015.

WYLLIE, M.; GREGORY, A.; GARDNER, L. Elastic wave velocities in heterogeneous and porous media. *Geophysics*, v. 21, n. 1, p. 41–70, jan. 1956.

ZHANG, J. Elastic wave modeling in fractured media with an explicit approach. *Geophysics*, v. 70, p. T75–T85, 2005.

ZHANG, J. Pore pressure prediction from well logs: Methods, modifications, and new approaches. *Earth-science reviews*, v. 108, n. 1–2, p. 50–63, set. 2011.

ZIMMERMAN, R. W. *Compressibility of Sandstones*. [S.l.]: Elsevier, 1990.